Journal of Medicinal Chemistry

pubs.acs.org/jmc

Article

Development of Ciprofibrate Platinum(IV) Nanodrugs as Antimetastatic Agents with COFs as Carriers

Shuaiqi Feng, Yan Chen, Zhifang Liu, Shilei Ji,* and Qingpeng Wang*

Cite This: J. Med. Chem. 2025, 68, 20340−20359

Read Online

ACCESS | Metrics & More | Article Recommendations | Supporting Information

ABSTRACT: Dysregulated cholesterol accumulation promotes tumor growth and metastasis. Herein, a series of ciprofibrate platinum(IV) conjugates with cholesterol-inhibiting effects was developed, and the transferrin-modified nanodrug Tf-PEG-COFs@Pt(IV) was prepared using COFs as the carrier. The nanodrug exhibited potent antiproliferative and antimetastatic activities both *in vitro* and *in vivo*. The transferrin moiety significantly enhanced the tumor-targeting ability of the nanodrug. The platinum core induced serious DNA damage, leading to an increased expression of γ-H2AX and p53. Mitochondria-mediated apoptosis occurred via the Bcl-2/Bax/caspase-3 cascade. Notably, cholesterol accumulation was inhibited by the ciprofibrate ligand through promoting PPAR-α expression and further regulating the LDLR/ACAT1/ABCA1 signaling. The nanodrug effectively reversed the epithelial-mesenchymal transition by inhibiting the PI3K/AKT/mTOR pathway and reversing the hypoxic microenvironment. Furthermore, antitumor immunity was enhanced by elevating the density of $CD3^+$ and $CD8^+$ T cells and triggering macrophage polarization from the M2 to M1 phenotype in tumors.

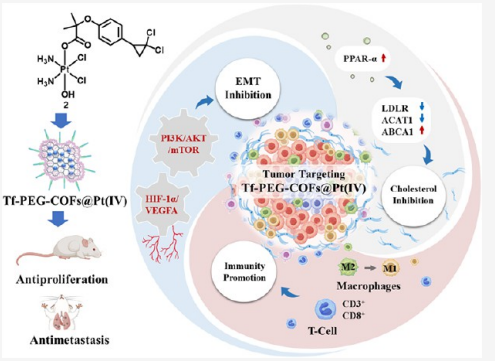

INTRODUCTION

Cancer remains one of the most formidable threats to human health, particularly with metastatic cancers accounting for over 90% of oncology-related deaths.[1,2] Conventional platinum(II) drugs, such as cisplatin (CDDP), carboplatin (CBP), and oxaliplatin (OXP), have long served as cornerstones for cancer treatments.[3,4] However, these drugs exhibit rather limited antimetastatic efficacy in the clinic. Platinum(IV) conjugates, as prodrugs of platinum(II) drugs with an octahedral structure, afford a promising scaffold for the design of novel platinum conjugates. The incorporation of various bioactive ligands into the platinum(IV) system has been proven to be a meaningful approach for developing novel platinum conjugates as potent antimetastatic agents.[5−7]

The epithelial-mesenchymal transition (EMT) process serves as a pivotal driver of tumor metastasis, endowing cancer cells with invasive properties, while also fostering immunosuppressive microenvironments and drug resistance.[8−10] Dysregulated accumulation of cholesterol has emerged as a critical hallmark of aggressive malignancies, providing essential building blocks for membrane synthesis during cell proliferation and migration.[11−14] Increasing evidence has indicated that cholesterol promotes tumorigenesis, cancer progression, and metastasis through multiple regulatory effects, such as immune response, ferroptosis, autophagy, cell stemness, and the DNA damage response.[15,16] Notably, high levels of cholesterol in tumors can initiate the PI3K/AKT/mTOR pathway and further drive the EMT process.[17] Meanwhile, aberrant cholesterol accumulation is also tightly associated with the formation of a hypoxic tumor microenvironment (TME), which significantly promotes EMT.[18−20] Accordingly, targeting cellular cholesterol accumulation appears to be a promising strategy for inhibiting EMT and further suppressing tumor proliferation and metastasis.

The peroxisome proliferator-activated receptor (PPAR) agonists are effective in reducing cholesterol levels by modulating cascades involving the biosynthesis, metabolism, and transport of sterols.[21,22] Fibrate drugs, as promising PPAR agonists, could regulate cholesterol metabolism and further display antitumor effects. Recently, fenofibrate was introduced into a platinum(IV) system to form hybrids **I**−**IV** (Figure 1), which displayed promising antitumor activities both *in vitro* and *in vivo*.[23,24] Mechanistic investigations evidenced that these conjugates promoted cholesterol efflux from tumors by activating PPAR-α and modulating cholesterol-related proteins LDLR, ACAT1, and ABCA1, and further destroyed membrane integrity to promote apoptosis synergistically with the DNA injury function from the platinum core. However, the potential of fibrate platinum(IV) hybrids in reversing EMT and suppressing tumor metastasis still warrants further inves-

Received: May 22, 2025
Revised: July 28, 2025
Accepted: September 10, 2025
Published: September 17, 2025

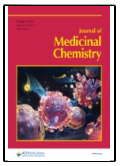

https://doi.org/10.1021/acs.jmedchem.5c01395
J. Med. Chem. 2025, 68, 20340−20359

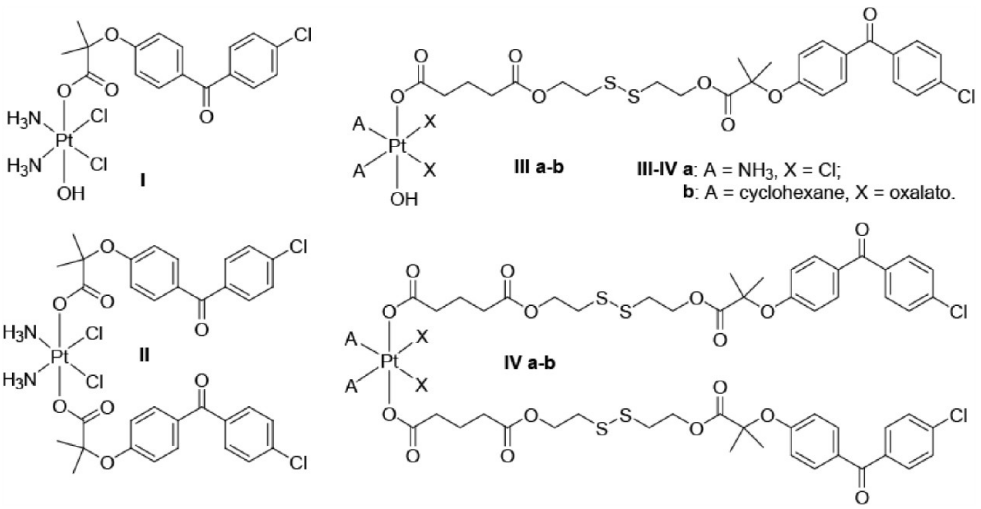

Figure 1. Structures of fenofibrate platinum(IV) hybrids **I**–**IV**.

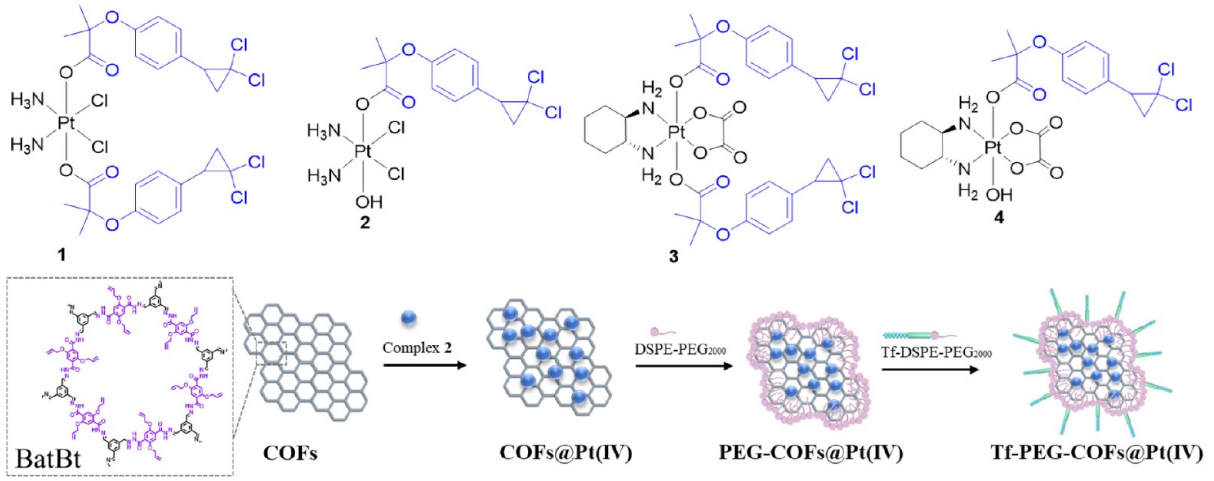

Figure 2. Structures of CF platinum(IV) hybrids **1**–**4** and the nanodrugs.

tigation. Inspired by these observations, ciprofibrate (CF), another promising PPAR-α agonist with a long half-life *in vivo,* was incorporated into a platinum(IV) system, and a new series of CF platinum(IV) conjugates **1**–**4** were prepared to further explore the potential of fibrate platinum(IV) conjugates as antimetastasis agents (Figure 2).

Nanodrug delivery systems (NDDS) have attracted remarkable attention for their potential to improve solubility and reduce the toxic effects of free drugs.[25,26] Numerous carriers for NDDS have been developed over the past decade.[27,28] Covalent organic frameworks (COFs), as a type of precisely constructed polymer with defined organic building blocks, have garnered considerable interest due to their multiple advantages over classical NDDS materials.[29−31] COFs, with their large microporous and porous aromatic frameworks, enable high loading of chemotherapeutics. Additionally, the lipophilic cavity in COFs affords a lipophilic environment for platinum(IV) complexes, effectively preventing their reduction in biological media prior to release. Platinum(IV) nanodrugs using COFs as carriers have not yet been investigated, and they are highly worthy of further exploration as potential antitumor agents. Herein, a COF, BatBt (2,5-bis(allyloxy)terephthalohydrazide-1,3,5-benzenetricarboxaldehyde), with hydrazone linker groups, was selected as the carrier for platinum(IV) conjugates[32] owing to the acid-cleavable characteristics of the hydrazone bond in the micellar material, which would favor the release of the active ingredient from nanodrugs in the acidic TME.[33,34]

Thereby, the nanoparticles COFs@Pt(IV) loading CF platinum(IV) conjugate with BatBt as the carrier were prepared to explore the potential of COFs in loading platinum(IV) complexes. However, the intrinsic limitations of COF materials, including low water solubility, nonspecific tumor targeting, and low cell-membrane permeability, were not overcome in such a nanoagent. Accordingly, DSPE-PEG_{2000} was introduced, and the nanoparticles PEG-COFs@Pt(IV) were prepared. Subsequently, the protein transferrin (Tf) was incorporated as a targeting motif to enhance tumor-targeting properties, and the nanodrug Tf-PEG-COFs@Pt(IV) was designed. The structures of the new conjugates **1**–**4** were characterized by ^{1}H NMR, ^{13}C NMR, and mass spectra. All complexes were over 95% pure, as determined by HPLC. The antiproliferative and antimetastatic activities of CF platinum(IV) conjugates and the nanodrugs were evaluated both *in vitro* and *in vivo*. Finally, their potential antitumor mechanisms were investigated.

https://doi.org/10.1021/acs.jmedchem.5c01395
J. Med. Chem. 2025, 68, 20340−20359

Scheme 1. Synthetic Route of Platinum(IV) Complexes 1−4

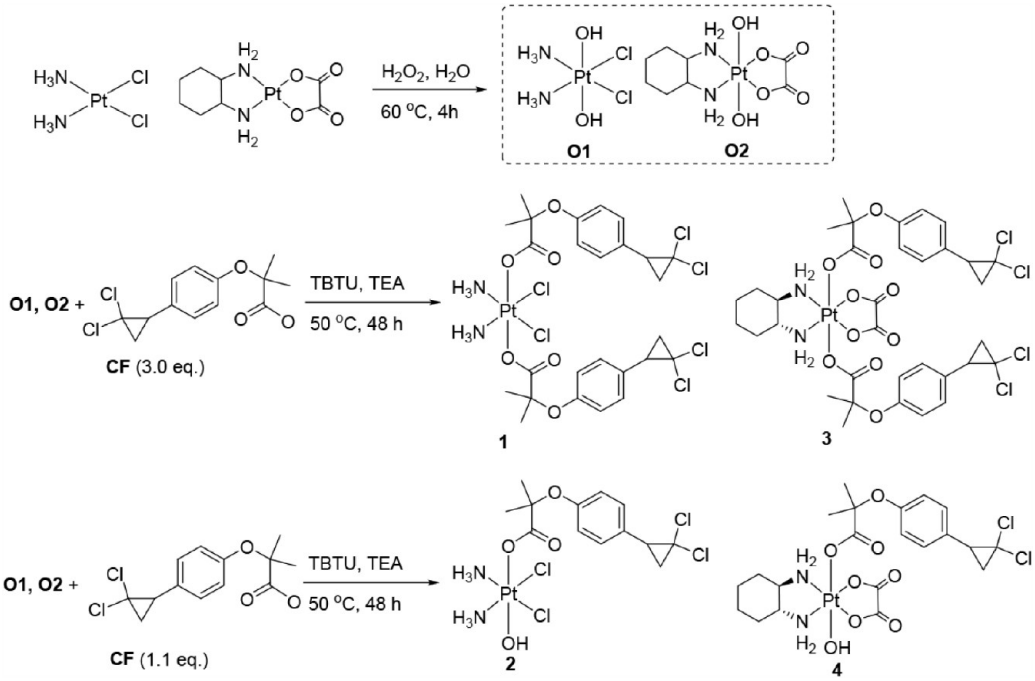

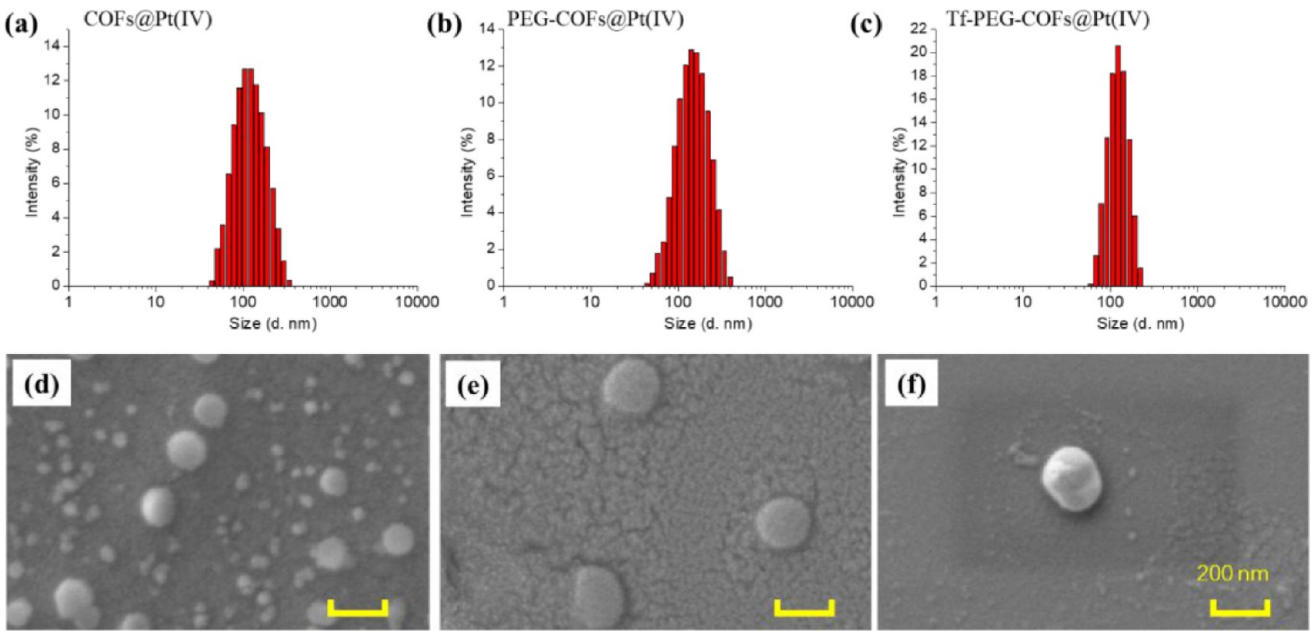

Figure 3. Particle size distribution was determined by DLS and SEM: (a, d) COFs@Pt(IV); (b, e) PEG-COFs@Pt(IV); (c, f) Tf-PEG-COFs@Pt(IV).

RESULTS AND DISCUSSION

Preparation and Characterization of CF Platinum(IV) Conjugates. The preparation of CF platinum(IV) hybrids began with the oxidation of CDDP and OXP using hydrogen peroxide, following published procedures,[35−38] which yielded oxoplatins **O1** and **O2** with dual hydroxyl axial ligands (Scheme 1). Subsequently, the condensation of oxoplatins **O1** and **O2** with 3.0 equiv of CF in the presence of N,N,N′,N′-tetramethyl-O-(benzotriazol-1-yl)uronium tetrafluoroborate (TBTU) and N,N,N-triethylamine (TEA) produced dual CF platinum(IV) complexes **1** and **3** in yields of 57.7% and 53.1%, respectively. Meanwhile, the conjunction of oxoplatins **O1** and **O2** with 1.1 equiv of CF afforded mono CF platinum(IV) complexes **2** and **4** in yields of 23.2% and 31.4%.

Preparation and Characterization of Nanoparticles. To screen out the candidate complex for nanodrug preparation, the antitumor activities of conjugates **1−4** were measured by an MTT assay (see the Antiproliferative Activities *In Vitro*), and the CDDP-derived conjugate **2** with a mono CF ligand exhibited the most promising activity. Thus, it was further utilized to prepare the nanodrug. The loading of conjugate **2** into COFs afforded COFs@Pt(IV) (97.2 ± 1.4 nm, PDI = 0.48 ± 0.03, ζ = −14.07 ± 0.85) (Figure 3). Subsequently, further encapsulation with DSPE-PEG$_{2000}$

https://doi.org/10.1021/acs.jmedchem.5c01395
J. Med. Chem. 2025, 68, 20340−20359

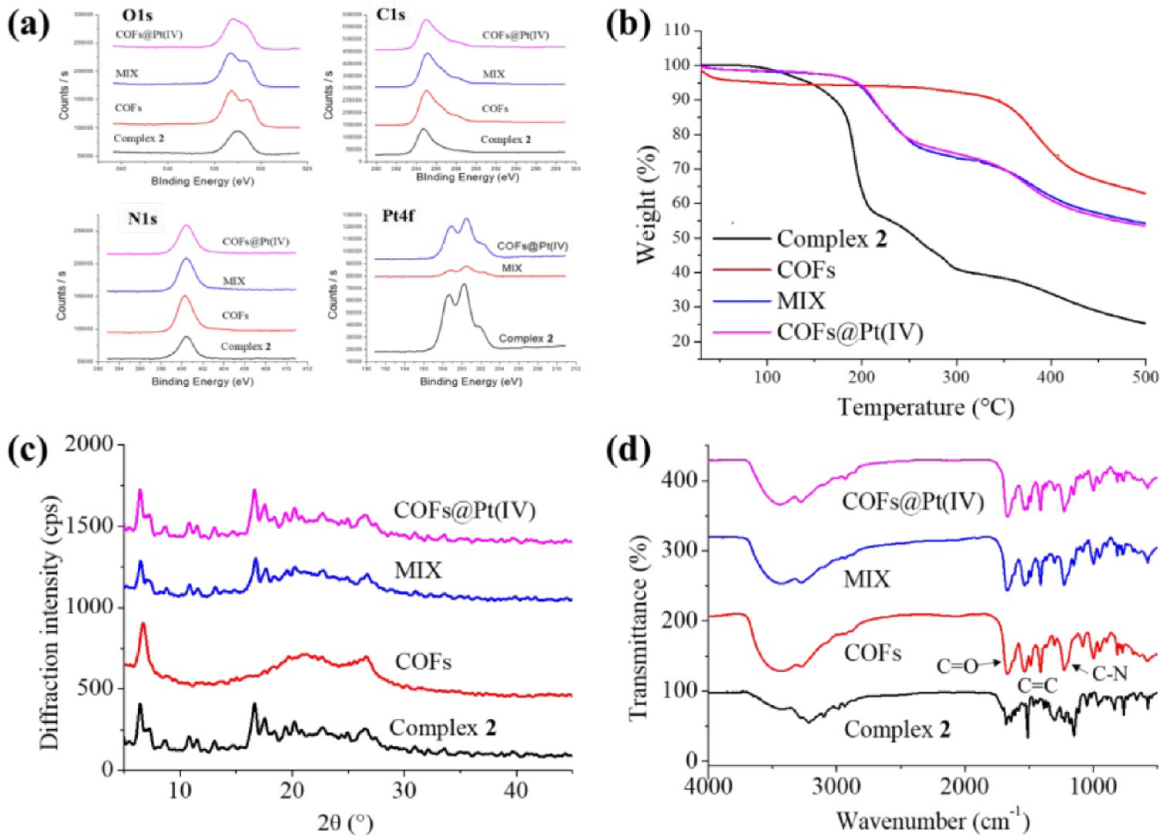

Figure 4. Characterization of complex **2**, COFs, the mixture of complex **2** with COFs (MIX), and the nanoparticles COFs@Pt(IV) was performed. (a) XPS spectra of the O 1s, C 1s, N 1s, and Pt 4f regions. (b) TGA spectra. (c) PXRD spectra. (d) IR spectra.

generated the nanoparticles PEG-COFs@Pt(IV) (106.0 ± 7.7 nm, PDI = 0.46 ± 0.02, ζ = −14.34 ± 0.51). Coincubation of Tf-DSPE-PEG_{2000} with PEG-COFs@Pt(IV) produced the tumor targeting nanodrug Tf-PEG-COFs@Pt(IV) (120.5 ± 2.7 nm, PDI = 0.62 ± 0.01, ζ = −20.5 ± 0.42). The binding ratio of Tf, as determined by the BCA kit, was 82.6%, which is expected to improve the tumor-targeting properties of the nanoparticles. The platinum content in COFs@Pt(IV), PEG-COFs@Pt(IV), and Tf-PEG-COFs@Pt(IV) was measured using an Atomic Absorption Spectrometry (AAS) assay to determine the concentration of the active ingredient in the nanodrugs, which were subsequently applied in biological evaluations. The morphology of the nanoparticles was further characterized by scanning electron microscopy (SEM, Figure 3). The nanoparticles exhibited spherical nanostructures. As expected, the Tf-DSPE-PEG_{2000} and PEG-COFs@Pt(IV) showed relatively larger diameters than COFs@Pt(IV) in the SEM images, which was primarily attributed to the encapsulation by the DSPE-PEG_{2000} layer.

The binding interactions of active ingredient 2 with COFs are important for understanding the encapsulation of the platinum(IV) complex with the carrier. Thus, the nanoparticles COFs@Pt(IV) were characterized by several instrumental techniques, including X-ray Photoelectron Spectroscopy (XPS), thermogravimetric analysis (TGA), PXRD, and FTIR, with free complex **2** and COFs, as well as the mixture of **2** with COFs (MIX) as references. The presence of Pt 4f in the XPS spectrum of COFs@Pt(IV) (Figures 4a and S1) indicated the loading of active ingredient **2** by the carrier COFs. Then, the variation of the binding energy, especially for the O 1s and C 1s in COFs@Pt(IV) in comparison with complex **2** and COFs, as well as the MIX groups, demonstrated the changes in their electron cloud density, which indicated the interactions between complex **2** and COFs in the nanoparticles. The TGA results in Figure 4b further validated the drug-loading capacity of COFs, as a significant weight loss (about 20%) was observed in COFs@Pt(IV) at about 197.56 °C, which was assigned to the degradation of the loaded active ingredient **2**. The PXRD spectra (Figure 4c) of COFs@Pt(IV) closely matched those of the original particles of complex **2** and COFs. Notably, slight shifts of the peaks at 8.72°, 16.68°, and 26.44° for COFs@Pt(IV) were observed after drug loading in comparison with the MIX group, probably corresponding to a minor expansion of the pore diameter during the course of complex **2** loading.[39,40] Slight shifts of IR signals (Figure 4d) for C═O, C═C, and C−N groups were also observed in COFs@Pt(IV) in comparison with those of complex **2** and COFs. These findings revealed that weak interactions between complex **2** and carrier COFs existed in the nanoparticles COFs@Pt(IV), which were favorable for the loading of the active ingredient into the carriers.

Then, the stability of Tf-PEG-COFs@Pt(IV) was monitored for 7 days by evaluating the particle size using DLS. The results in Figure S2 revealed that both PEG-COFs@Pt(IV) and Tf-PEG-COFs@Pt(IV) exhibited good stability under 4 °C storage, with the particle size fluctuating within a relatively acceptable range. Meanwhile, the size of the nanoparticles in COFs@Pt(IV) increased to 230.8 ± 14.6 nm after 7 days of storage. These findings indicate that the modification of COFs nanoparticles with DSPE-PEG_{2000} effectively improves their storage stability.

https://doi.org/10.1021/acs.jmedchem.5c01395
J. Med. Chem. 2025, 68, 20340−20359

Table 1. Antiproliferative Activities of CF Platinum(IV) Complexes 1−4 and the Nanoparticles PEG-COFs@Pt(IV) and Tf-PEG-COFs@Pt(IV) Against Four Tumor Cell Lines with CF, CDDP-CF, CDDP, and OXP as References[a]

Agents	4T1	A549	A549R	RF[b]	HepG2	LO2	SI[c]
1	4.52 ± 0.37	3.17 ± 0.22	4.63 ± 0.89	1.46	2.65 ± 0.46	1.85 ± 0.24	0.70
2	1.44 ± 0.24	0.72 ± 0.14	0.33 ± 0.09	0.46	0.94 ± 0.12	0.83 ± 0.13	0.88
3	17.62 ± 2.56	12.60 ± 2.47	10.8 5± 1.06	0.86	14.61 ± 1.29	16.25 ± 2.66	1.11
4	4.22 ± 0.35	1.79 ± 0.29	5.56 ± 0.80	3.11	8.98 ± 0.71	14.28 ± 2.07	1.59
PEG-COFs@Pt(IV)	0.61 ± 0.05	0.26 ± 0.03	0.41 ± 0.07	1.58	0.24 ± 0.04	0.91 ± 0.04	3.79
Tf-PEG-COFs@Pt(IV)	0.19 ± 0.04	0.12 ± 0.04	0.05 ± 0.01	0.42	0.12 ± 0.01	0.64 ± 0.09	5.33
CF	>50	>50	>50	ND[d]	>50	>50	ND
CDDP	4.79 ± 0.36	3.86 ± 0.30	23.75 ± 0.16	6.15	2.57 ± 0.42	1.78 ± 0.16	0.69
OXP	22.89 ± 3.71	21.87 ± 2.31	30.47 ± 2.24	1.39	41.69 ± 3.99	37.10 ± 1.67	0.89
CDDP-CF[e]	7.55 ± 0.79	4.79 ± 0.27	15.10 ± 2.33	3.15	5.94 ± 0.69	7.89 ± 0.93	1.33

[a]Cells were treated with drugs for 48 h and the half-maximal inhibitory concentrations (IC50, μM) were determined based on three parallel experiments . [b]RF: resistance factor, RF = IC_{50}(A549R)/IC_{50}(A549). [c]SI: selective index, SI = IC_{50}(LO2)/IC_{50}(HepG2). [d]CDDP-CF: a mixture of CDDP with CF in a molar ratio of 1:1. [e]ND: not tested or not calculated.

Release Behavior of Complex 2 from Nanoparticles and Further Reduction in TME. The release behavior of complex **2** from the nanodrug Tf-PEG-COFs@Pt(IV) was studied in PBS medium and compared with the injection of free complex **2** (dissolved in PBS containing 5% DMF). The concentration of complex **2** in the release culture was determined by using an AAS assay. Results in Figure S3 demonstrated that the active ingredient **2** was released from Tf-PEG-COFs@Pt(IV) in a sustained manner, whereas free complex **2** exhibited a burst release of up to 90% within 6 h. The long-term drug release behavior of Tf-PEG-COFs@Pt(IV) would prolong tumor exposure to chemotherapeutics and further improve antitumor activities.

The platinum(IV) complexes were expected to be stable in the medium during storage and to undergo reduction easily in the reducing TME in the body. Thus, the stability of active ingredient **2** in PBS and its reduction properties in reducing media were assessed using HPLC. The results in Figure S4 demonstrated that conjugate **2** remained stable for at least 48 h in PBS. It was then easily reduced under reducing conditions (PBS with reducing AsA, 1 mM) (Figure S5), as evidenced by the shrinkage of the peak for complex **2** and the gradual increase of the peak for CF. Accordingly, the CF platinum(IV) conjugate **2** remained stable during storage and transport in the biological medium, and then it would undergo reduction in the reducing TME.

Antiproliferative Activities *In Vitro*. The antiproliferative activities of CF Pt(IV) complexes **1**−**4**, nanoparticles Pt(IV), and Tf-PEG-COFs@Pt(IV) were evaluated using the MTT assay against four tumor cell lines: human lung carcinoma (A549), cisplatin-resistant lung carcinoma (A549R), murine breast cancer (4T1), and human hepatoma (HepG2). The normal human liver cell line (LO2) was evaluated for toxicity assessment. Platinum(II) drugs CDDP and OXP were applied as references. Additionally, CF and a physical mixture of CDDP with CF (CDDP-CF) were also tested.

It was demonstrated in Table 1 that the CF platinum(IV) complexes **1**−**4** displayed potent antitumor activities against all tested tumor cell lines. Specifically, the structure−activity relationship (SAR) analysis revealed that the platinum core had a remarkable influence on antitumor performance, with conjugates **1** and **2** containing a CDDP core showing more potent antitumor activity than the OXP-derived ones, **3** and **4**. Furthermore, the ligands also exerted significant influence on antitumor potency, as complexes **2** and **4** with a mono CF ligand were significantly more effective than the dual CF ones, **1** and **3**. This trend was similar to that observed in Fenofibrate platinum(IV) complexes.[23,24] The mono CF platinum(IV) complex **2** with a CDDP core, demonstrated the most potent antitumor activity, with IC_{50} values below 1.44 μM, proving to be even more effective than the reference drugs CDDP and OXP. Notably, the free ligand CF showed negligible activity against tumor cells (IC_{50} > 50 μM), and the physical mixture of CF with CDDP (CDDP-CF) resulted in no significant enhancement of antitumor activity compared to CDDP alone. Considering the improved antitumor activities of CF platinum(IV) conjugates compared to those of CDDP-CF, the conjugation of functional ligands into the platinum(IV) system to form multifunctional molecules seemed critical for developing potent antitumor drugs.

The preparation of nanoparticles with the potent complex **2** as the active ingredient further enhanced the antitumor performance. PEG-COFs@Pt(IV) reduced the IC_{50} values to 0.24−0.61 μM. Notably, Tf-PEG-COFs@Pt(IV) exhibited significantly better antitumor efficacy than PEG-COFs@Pt(IV), with IC_{50} values in the range of 0.05−0.19 μM. The improvement was probably attributed to the enhanced tumor-targeting ability conferred by the Tf motif, which facilitated more efficient accumulation of nanoparticles in tumor cells (Figure S10b).

Furthermore, the nanodrug Tf-PEG-COFs@Pt(IV) showed promise in overcoming drug resistance by reducing the resistance factor (RF) to 0.42, which is significantly lower than that of CDDP (RF = 6.15) and comparable to the active ingredient **2** (RF = 0.46). More importantly, Tf-PEG-COFs@Pt(IV) effectively reduced the toxicity of complex **2** to normal cells, exhibiting a selective index (SI) of 5.33, which is significantly higher than that of free conjugate **2** (SI = 0.88) and reference drugs CDDP, OXP, and CDDP-CF (SI = 0.69−1.33). It also outperformed PEG-COFs@Pt(IV) (SI = 3.79), indicating that incorporating the tumor-targeting Tf motif into the nanosystem significantly reduced the toxicity of drugs *in vitro*.

Antitumor Activities *In Vivo*. To assess the *in vivo* antitumor efficacy, CF platinum(IV) complex **2** and the nanoparticles PEG-COFs@Pt(IV) and Tf-PEG-COFs@Pt(IV) were evaluated in female BALB/c mice bearing 4T1 tumors. CDDP and CDDP-CF were applied as positive controls, while media-treated mice were used as the blank group. As depicted in Figure 5a, the compounds were administered intra-

https://doi.org/10.1021/acs.jmedchem.5c01395
J. Med. Chem. 2025, 68, 20340−20359

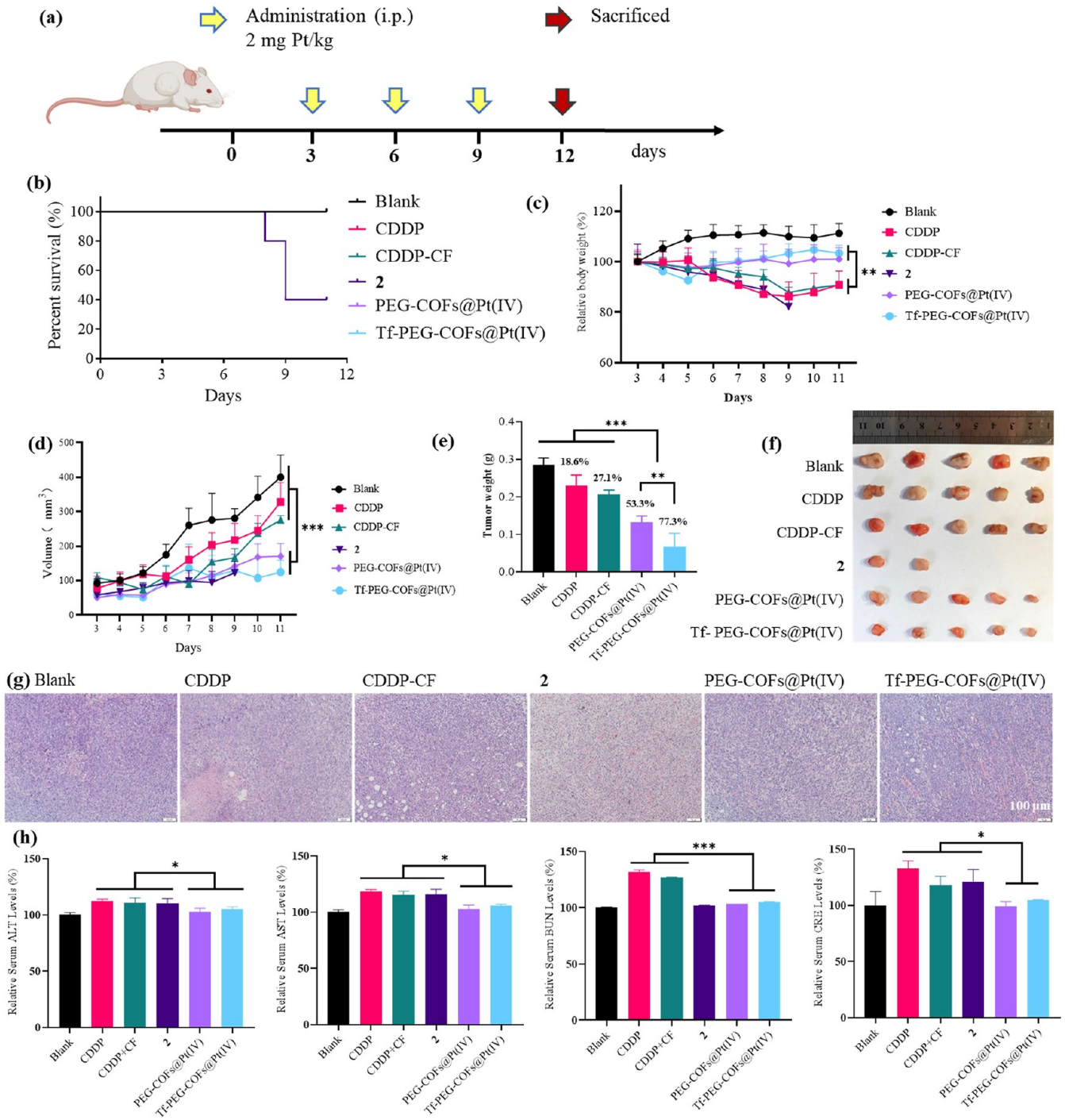

Figure 5. *In vivo* antitumor activities of CDDP, CDDP-CF, complex **2**, PEG-COFs@Pt(IV), and Tf-PEG-COFs@Pt(IV) were assessed in 4T1 tumors in BALB/c mice (n = 5). (a) Schematic illustration of the experimental design. (b) Survival analysis of mice during the treatment. (c) Relative body weight of the mice during the treatment. (d) Tumor growth as a function of time. (e) Tumor weight of each group at the end of the experiment. The TGI of the tested drugs in comparison with the blank group was depicted above the column [TGI = (1 − tumor weight of the drug-treated group/tumor weight of the saline group) × 100%]. (f) Image of tumors after the mice sacrificed. (g) H&E staining of tumor tissues. (h) ELISA analysis of ALT, AST, BUN, and CRE in blood. *p < 0.05, **p < 0.01, ***p < 0.001.

peritoneally (i.p.) at a dosage of 2 mg of Pt/kg on days 3, 6, and 9 following tumor inoculation. On day 12, the mice were euthanized for the excision of tumors and the collection of major organs, including the heart, liver, spleen, lungs, and kidneys. Subsequently, immunohistochemical (IHC) analysis was conducted to examine protein expression within the tumor tissues.

First, the systemic toxicity was evaluated by examining the survival rate and changes in body weight. The free complex **2** led to a significant reduction in the survival rate to 40% in 9 days, which was even more toxic than platinum(II) drugs such as CDDP (Figure 5b). Meanwhile, the preparation of nanodrugs dramatically decreased the toxicity of complex **2**, so that PEG-COFs@Pt(IV) and Tf-PEG-COFs@Pt(IV)

https://doi.org/10.1021/acs.jmedchem.5c01395
J. Med. Chem. 2025, 68, 20340−20359

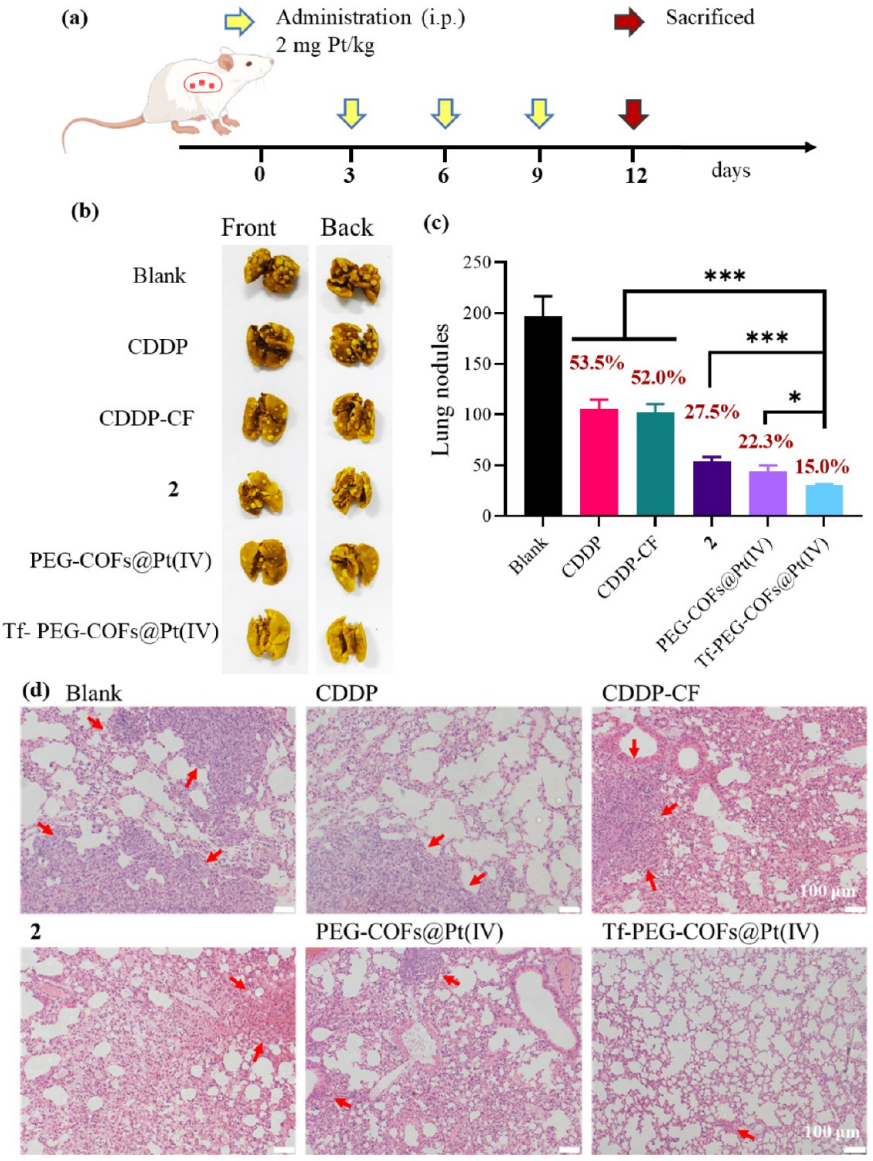

Figure 6. Pulmonary metastasis inhibition properties of CDDP, CDDP-CF, complex **2**, PEG-COFs@Pt(IV), and Tf-PEG-COFs@Pt(IV) against 4T1 tumors *in vivo* (n = 5). (a) Schematic illustration of the experimental design. (b) Representative photographs of the front and back sides of lungs from each group at the end of the experiment. (c) Lung nodules in each group. The inhibition rate compared with the blank group was depicted above the column. (d) H&E staining of lung metastasis nodules. Nodules were indicated by red arrows. *p < 0.05, ***p < 0.001.

resulted in no deaths of mice during the experiment. Furthermore, these nanoparticles induced a smaller reduction in body weight compared to both CDDP and the CDDP-CF mixture (p < 0.01, Figure 5c). Hematoxylin−eosin staining (H and E) examination of the liver, spleen, and kidney revealed no significant differences between the nanodrug-treated groups and the blank group (Figure S6). The liver and kidney injuries are usually associated with the toxicities of platinum (II) drugs. Here, the ALT and AST levels associated with liver damage, as well as BUN and CRE levels associated with kidney damage, were measured by using ELISA assays. Results depicted in Figure 5h showed that complex **2** induced higher levels of ALT, AST, and CRE than the blank group, which were similar to those of CDDP, demonstrating its toxicity toward the liver and kidney. These findings might be the primary reasons for the toxicity of free compound **2**, which further led to the death of the mice. Meanwhile, the nanodrugs PEG-COFs@Pt(IV) and Tf-PEG-COFs@Pt(IV) exhibited negligible impacts on these factors, which were significantly lower than those of free complex **2**, CDDP, and CDDP-CF (p < 0.05). This indicated that the construction of nanodrugs was effective in reducing the *in vivo* toxicities of the active ingredient CF platinum(IV) complex **2**.

Encouragingly, the nanodrugs PEG-COFs@Pt(IV) and Tf-PEG-COFs@Pt(IV) demonstrated substantially improved antigrowth effects *in vivo* compared to both free complex **2** and platinum (II) drugs (Figure 5d−f). PEG-COFs@Pt(IV) and Tf-PEG-COFs@Pt(IV) achieved high tumor growth inhibition rates (TGI) of 53.3% and 77.3%, respectively, which were significantly superior to those of CDDP and the mixture CDDP-CF (TGI = 18.6%, 27.1%, p < 0.001). This trend was primarily consistent with their *in vitro* antitumor performance. The H and E staining results in Figure 5g further evidenced their antitumor efficacy, as pronounced cellular degeneration, necrosis, and nuclear dispersion were observed in the PEG-COFs@Pt(IV) and Tf-PEG-COFs@Pt(IV)

https://doi.org/10.1021/acs.jmedchem.5c01395
J. Med. Chem. 2025, 68, 20340−20359

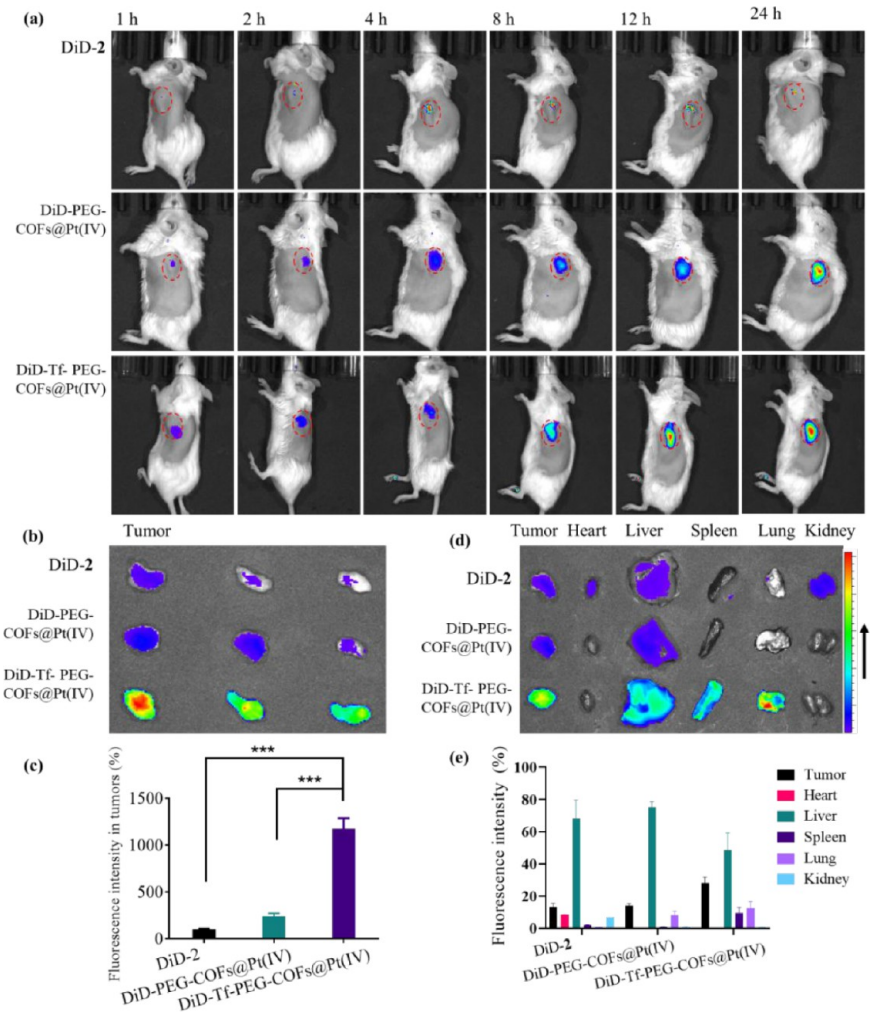

Figure 7. Biodistribution and tumor-targeting studies of DiD-labeled nanoparticles DiD-PEG-COFs@Pt(IV) and DiD-Tf-PEG-COFs@Pt(IV), as well as the mixture of DiD with free complex **2** (DiD-**2**) conducted *in vivo* (n = 3). (a) Mice bearing 4T1 tumors were injected with the DiD-labeled agents (i.v.) followed by dynamic scanning using an IVIS optical imaging system at 1, 2, 4, 8, 12, and 24 h postinjection. (b,c) The relative fluorescence intensity of tumors at the end of the experiment. (d,e) *Ex vivo* images and the distribution of drugs in tissues, including tumor, heart, liver, spleen, lung, and kidney (Relative fluorescence intensity = (Fluorescence intensity in specified tissues/Fluorescence intensity in all tissues, including tumor, heart, liver, spleen, lung, and kidney) × 100%). ***p < 0.001.

groups, paralleling those in complex **2**, CDDP, and CDDP-CF-treated tumors. Moreover, the Tf-PEG-COFs@Pt(IV) with a Tf motif showed even higher antitumor potency than the PEG-COFs@Pt(IV) group (p < 0.01), which was attributed to the elevated tumor-targeting properties (see "Tumor Targeting Properties *In Vivo*" section).

Subsequently, the survival rate of mice following drug treatments was evaluated to determine the impact of the drugs on the survival period of mice, and the results are given in Figure S7. It was observed that the survival rate of mice treated with complex **2** decreased rapidly after drug administration, similar to the trend shown in Figure 5b, which was probably attributed to its severe toxicities. In contrast, the nanodrugs PEG-COFs@Pt(IV) and Tf-PEG-COFs@Pt(IV) significantly mitigated the *in vivo* toxicities in comparison with free complex **2**. Moreover, the nanodrugs extended the survival period of the mice remarkably compared with complex **2**, blank, CDDP, and CDDP-CF groups. Notably, the survival rate of mice in the Tf-PEG-COFs@Pt(IV) group remained at 70% on day 28, surpassing that of the PEG-COFs@Pt(IV) group (50.0%). Therefore, the tumor-targeting nanodrug Tf-PEG-COFs@Pt(IV) was promising in decreasing toxicities and prolonging the survival period *in vivo*, besides displaying satisfactory antigrowth properties.

Accordingly, the CF platinum(IV) nanodrugs with COFs as the carrier displayed promising antiproliferative efficacy *in vivo*, which were more potent and less toxic than the platinum(II) reference drug CDDP, the mixture CDDP-CF, and the free CF platinum(IV) complex **2**. Especially, Tf-PEG-COFs@Pt(IV) possessed the most attractive performance, mainly due to its promising tumor-targeting abilities.

Antimetastatic Activities *In Vitro* and *iln Vivo*. To assess the potential of Tf-PEG-COFs@Pt(IV) as antimetastatic agents, transwell and wound healing assays were employed for *in vitro* evaluation. The results presented in Figure S8 revealed that complex **2** and its nanodrugs, PEG-COFs@Pt(IV) and Pt(IV), effectively inhibited the migration of tumor cells compared to the blank, CDDP, and CDDP-CF groups (p < 0.001). Similar to the antiproliferative activities, Tf-PEG-COFs@Pt(IV) was even more promising than the free conjugate **2** (p < 0.01) and the nanodrug PEG-COFs@Pt(IV) (p < 0.001). Moreover, the wound healing rates shown in

https://doi.org/10.1021/acs.jmedchem.5c01395
J. Med. Chem. 2025, 68, 20340−20359

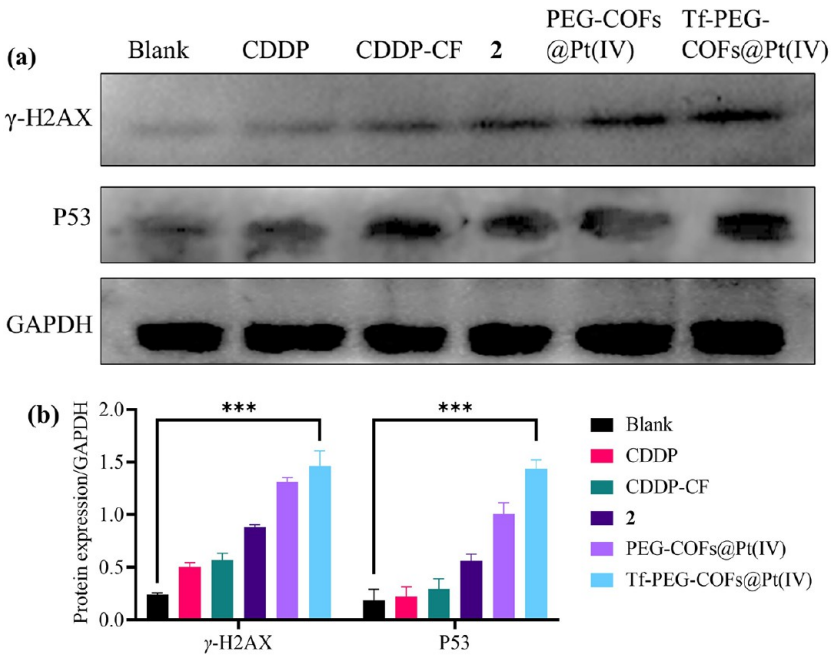

Figure 8. Western blot analysis of γ-H2AX and P53 in 4T1 cells treated with and without CDDP (3 μM), CDDP-CF (3 μM/3 μM), complex **2** (3 μM), PEG-COFs@Pt(IV) (3 μM), and Tf-PEG-COFs@Pt(IV) (3 μM) for 24 h at 37 °C. (a) Blots. (b) Relative gray intensity analysis. Relative gray intensity = (gray intensity of indicated protein)/(gray intensity of GAPDH). ***$p < 0.001$.

Figure S9 further evidence this trend. These findings indicate that Tf-PEG-COFs@Pt(IV) is potent in inhibiting the metastasis of tumor cells *in vitro*.

Then, its antimetastatic efficacy *in vivo* was further evaluated using pulmonary metastasis models. The 4T1 cells were injected intravenously (i.v.) via the tail vein. Subsequently, the drugs were administered intraperitoneally (i.p.) at a dosage of 2 mg of Pt/kg on days 3, 6, and 9 (Figure 6a). On day 12, the mice were euthanized. Lung tissues were collected, and the nodules on the surface of the lungs were counted. As shown in Figure 6b,c, the nanodrugs PEG-COFs@Pt(IV) and Tf-PEG-COFs@Pt(IV) effectively suppressed the number of nodules to 22.3% and 15.0% of the blank group, respectively, which were also lower than the free complex **2** (27.5%, $p < 0.001$) and the CDDP and CDDP-CF groups (53.5% and 52.0%, $p < 0.001$). Encouragingly, Tf-PEG-COFs@Pt(IV) also possessed the most promising antimetastatic potency *in vivo* that it reduced the migration rate to 15.0% of the blank group, which was even lower than PEG-COFs@Pt(IV) (22.3%, $p < 0.05$). This effect was probably attributable to its enhanced tumor-targeting capability owing to the presence of the Tf motif. Then, the H&E staining results (Figure 6d) further verified that fewer and smaller lung metastatic nodules were observed in the Tf-PEG-COFs@Pt(IV)-treated group than in the blank, CDDP, CDDP-CF, conjugate **2**, and nanodrug PEG-COFs@Pt(IV) groups, indicating its effective antimetastatic potency *in vivo*. In total, the *in vitro* and *in vivo* antimetastatic tests showed that the nanodrug Tf-PEG-COFs@Pt(IV) held significant promise for further development as a novel antimetastatic agent.

Tumor-Targeting Properties. The tumor-targeting properties were essential in influencing the antitumor performance of the chemotherapeutics. The uptake of platinum drugs in tumor cells was a key index for assessing their tumor-targeting abilities. Herein, the uptake of Tf-PEG-COFs@Pt(IV) in tumor cells *in vitro* and in tumor tissues *in vivo* was measured using the AAS assay. The results in Figure S10a indicated that Tf-PEG-COFs@Pt(IV) led to a high accumulation in tumor tissues, which was over 6.3 and 5.1 times higher than the CDDP and CDDP-CF groups ($p < 0.001$), respectively. Notably, its uptake level was also higher than that of the free complex **2** (2.8-fold, $p < 0.001$) and the nanodrug PEG-COFs@Pt(IV) (2.2-fold, $p < 0.001$). Furthermore, the uptake data in tumor cells *in vitro*, shown in Figure S10b displayed a similar trend, with Tf-PEG-COFs@Pt(IV) accumulating at a high level in 4T1 cells in contrast to CDDP, CDDP-CF, conjugate **2**, and PEG-COFs@Pt(IV) ($p < 0.001$).

To further validate the tumor-targeting properties of the Tf-modified nanodrug, an *in vivo* imaging system (IVIS) assay was conducted. Fluorescently labeled nanoparticles, DiD-PEG-COFs@Pt(IV) and DiD-Tf-PEG-COFs were synthesized with DiD as a fluorescent probe and subsequently administered to tumor-bearing BALB/c mice (i.v.). A mixture of DiD with conjugate **2** (DiD-**2**) was applied as a control. The fluorescence intensity of different groups at the tumor sites was monitored by using the IVIS optical imaging system. The results indicated that DiD-Tf-PEG-COFs@Pt(IV) exhibited a higher accumulation in tumor tissues compared to DiD-PEG-COFs@Pt(IV) and free DiD-**2** groups ($p < 0.001$) (Figure 7), which was attributed to the incorporation of the Tf motif. Drug distribution analysis in tumors and organs (heart, liver, spleen, lung, and kidney) demonstrated that DiD-Tf-PEG-COFs@Pt(IV) achieved a tumor accumulation rate of 28.2%, markedly higher than that of DiD-PEG-COFs@Pt(IV) (14.3%) and DiD-2 (13.2%). These results indicated that the nanodrug Tf-PEG-COFs@Pt(IV) could accumulate at tumor sites in a higher proportion, which would further exert a positive influence on increasing antitumor activities and decreasing toxicities.

Consequently, the findings from the uptake and IVIS assays confirmed that the tumor-targeting nanodrug Tf-PEG-COFs@Pt(IV) exhibited promising tumor-targeting potential both *in*

https://doi.org/10.1021/acs.jmedchem.5c01395
J. Med. Chem. 2025, 68, 20340−20359

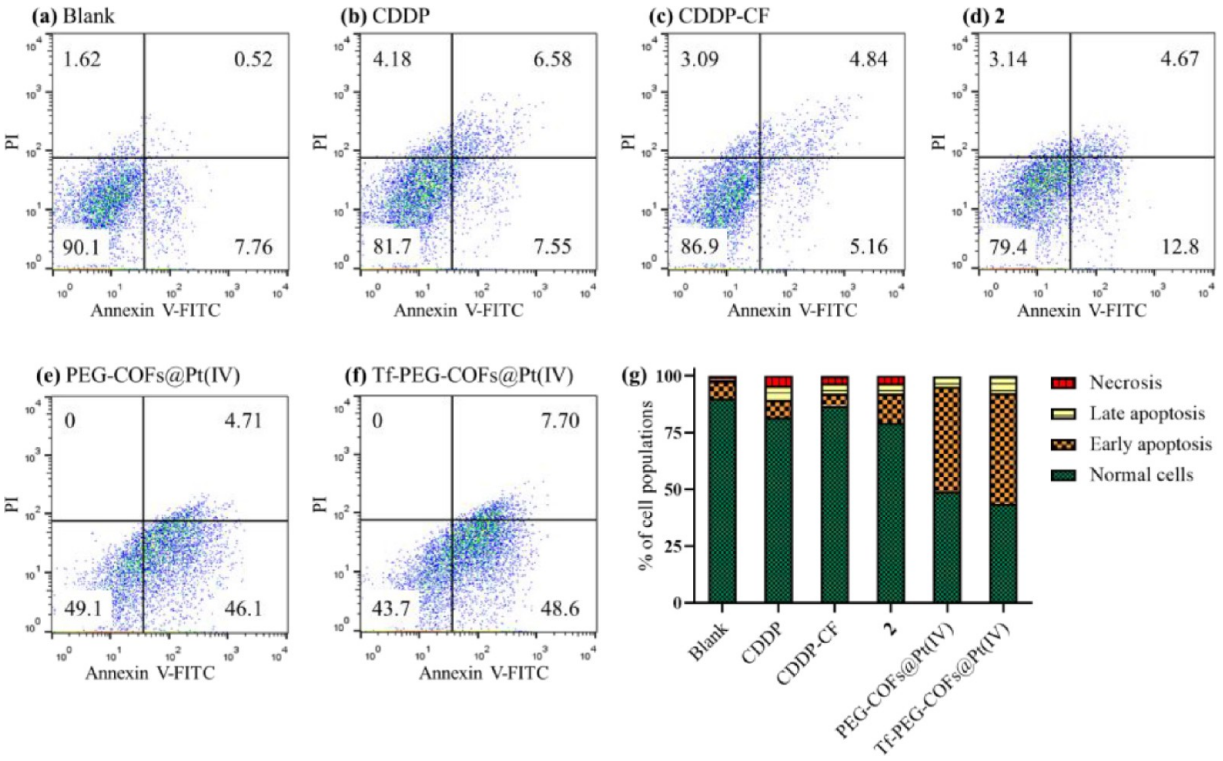

Figure 9. Quantification of apoptosis using an Annexin V-FITC/PI staining assay. The 4T1 tumor cells were incubated with and without platinum complexes for 24 h at 37 °C. (a) Blank. (b) CDDP (3 μM). (c) CDDP-CF (3 μM/3 μM). (d) Compound **2** (3 μM). (e) PEG-COFs@Pt(IV) (3 μM). (f) Tf-PEG-COFs@Pt(IV) (3 μM). (g) Stacking columns.

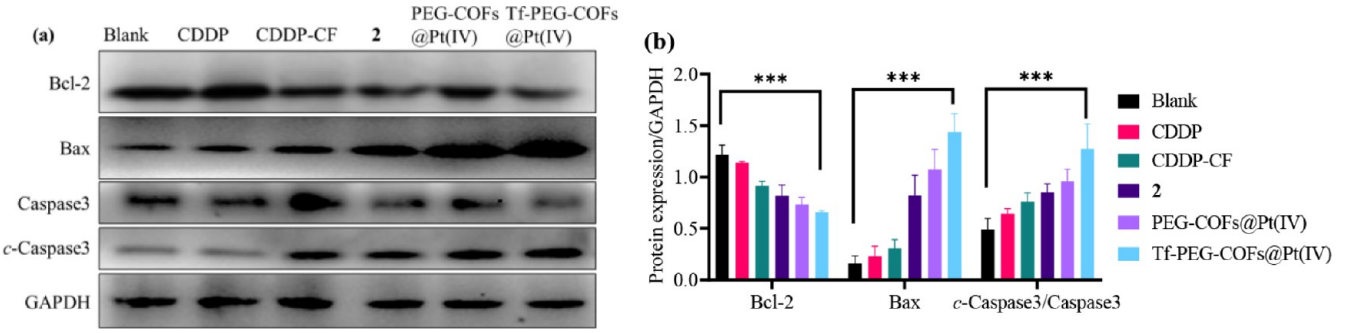

Figure 10. Western blot analysis of Bcl-2, Bax, caspase-3, and *c*-caspase-3 in 4T1 cells treated with and without CDDP (3 μM), CDDP-CF (3 μM/3 μM), compound **2** (3 μM), PEG-COFs@Pt(IV) (3 μM), and Tf-PEG-COFs@Pt(IV) (3 μM) for 24 h at 37 °C. (a) Blots. (b) Relative gray intensity analysis. ***$p < 0.001$.

vitro and *in vivo*, thereby leading to enhanced antitumor activity and reduced *in vivo* toxicity.

Induction of DNA Injury. The DNA damage was the critical mechanism by which platinum drugs killed tumor cells. To determine the DNA injury potency of Tf-PEG-COFs@Pt(IV), HPLC and Western blot assays were employed. As revealed in Figure S5, conjugate **2** was reduced to its platinum(II) form in a reducing environment. Subsequently, 5′-GMP was added as a DNA base model, and a solution containing complex **2**, AsA, and 5′-GMP was prepared and incubated for 48 h. The results in Figure S11 disclosed that a new peak corresponding to platinate GMP (verified by MS) emerged, indicating that the released platinum(II) moiety effectively bound to the DNA base and further induced severe DNA damage. Subsequently, Western blotting was used to detect the DNA damage indicator proteins γ-H2AX and P53. As shown in Figure 8, both γ-H2AX and P53 were significantly upregulated by Tf-PEG-COFs@Pt(IV) compared with the blank group ($p < 0.001$), which was similar to the results observed in the CDDP and CDDP-CF groups.

In summary, the active ingredient complex **2** of the nanodrug Tf-PEG-COFs@Pt(IV) induces severe DNA damage by binding to DNA after reduction, thereby further upregulating the expression of DNA damage marker proteins γ-H2AX and P53.

Induction of Mitochondria-Mediated Apoptosis. Apoptosis is an essential mechanism of cell death. Platinum drugs are typically potent in inducing apoptosis. In this study, an Annexin V-FITC/Propidium Iodide (PI) double-staining assay was applied to determine whether the antitumor efficacy of the nanodrug Tf-PEG-COFs@Pt(IV) was associated with apoptosis. As reflected in Figure 9, Tf-PEG-COFs@Pt(IV) effectively induced apoptosis in tumor cells (52.3%), which was more pronounced than the free conjugate **2** (17.4%) and

https://doi.org/10.1021/acs.jmedchem.5c01395
J. Med. Chem. 2025, 68, 20340−20359

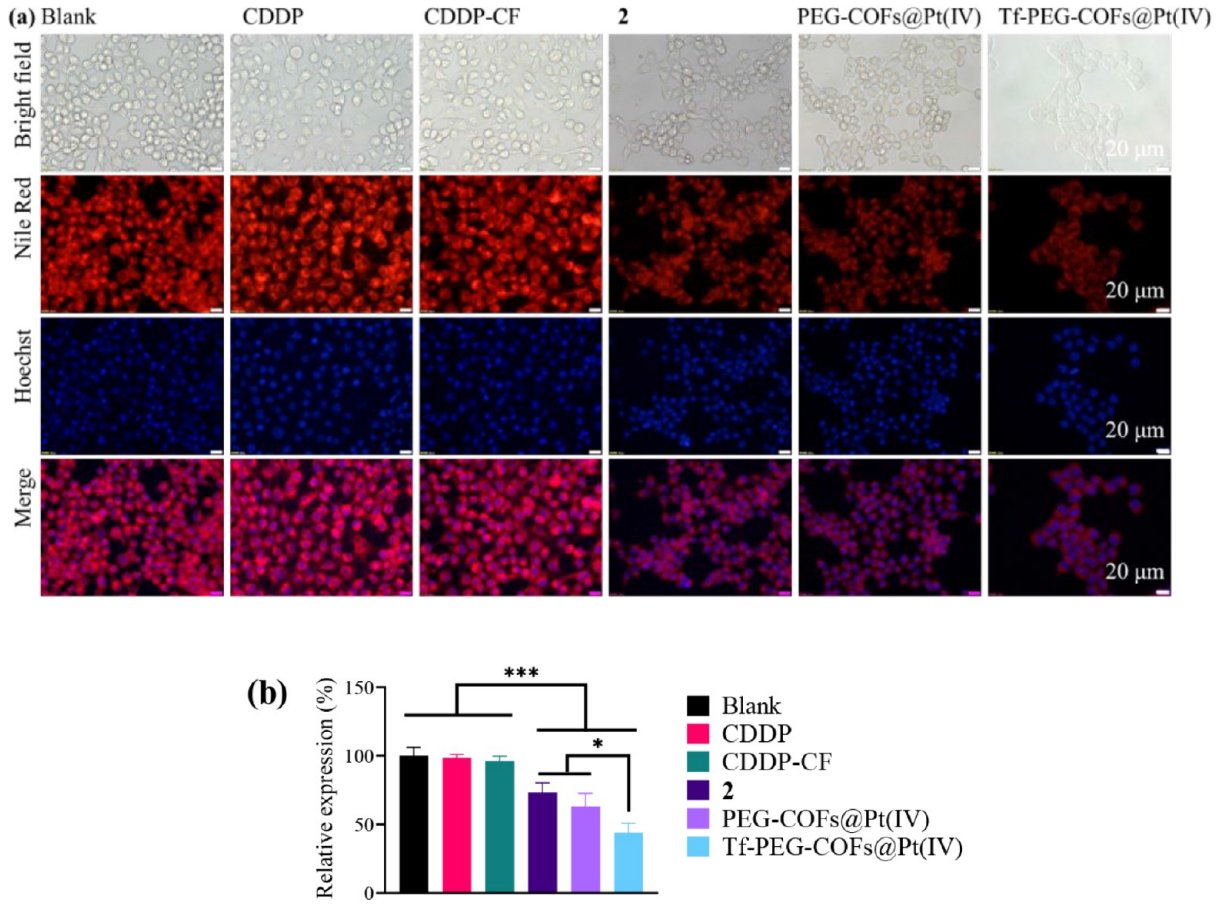

Figure 11. Lipid droplets in 4T1 cells stained with Nile red after treatment with each compound (1 μM) for 24 h. (a) Fluorescence images. Nile red: red, lipid droplets; Hoechst 33258: blue, nuclei. (b) Relative fluorescence intensity analysis of Nile red. Data were presented as mean ± SD (n = 3, *p < 0.05, ***p < 0.001).

the reference drugs CDDP (14.1%) and CDDP-CF (10.0%). These findings were largely consistent with the MTT assay results obtained *in vitro*. Mitochondria are widely recognized as vital cellular organelles in the regulation and induction of apoptosis. The collapse of mitochondrial membrane potential ($\Delta\Psi_m$) is a hallmark of apoptotic progression. As revealed in the JC-1 staining results (Figure S12), Tf-PEG-COFs@Pt(IV) also caused a significant loss of $\Delta\Psi_m$ (27.9%) compared to that of the blank group, which was greater than that of the PEG-COFs@Pt(IV) (19.8%), CDDP (14.1%), and CDDP-CF (10.3%) groups.

Subsequently, a Western blot assay was applied to detect the expression of proteins involved in the Bcl-2 cascades, which are primarily associated with mitochondria-mediated apoptosis (Figure 10). The key antiapoptotic protein Bcl-2 in tumor cells was suppressed by Tf-PEG-COFs@Pt(IV) in contrast to the blank group (p < 0.001), while the pro-apoptotic protein Bax was upregulated (p < 0.001). Furthermore, the cleavage of the apoptotic executioner protein caspase-3 was induced, and the ratio of *c*-caspase-3/caspase-3 increased significantly in the Tf-PEG-COFs@Pt(IV)-treated cells (p < 0.001).

Accordingly, the titled nanodrug Tf-PEG-COFs@Pt(IV) was potent in boosting apoptosis of tumor cells through the Bcl-2/Bax/caspase-3 pathway by causing significant mitochondrial damage.

Inhibition of Cholesterol Accumulation. High levels of cholesterol often occur in tumor cells. Excessive cholesterol can be converted into lipid droplets, which significantly drive the proliferation and aggression of tumor cells. CF, as a PPAR-α agonist, has been proven effective in promoting cholesterol metabolism. The nanodrug Tf-PEG-COFs@Pt(IV) is expected to provoke PPAR-α expression through the CF functional ligand, which would further lead to the efflux of cholesterol from the tumor cells.

To verify this hypothesis, lipid droplets in 4T1 tumor cells were stained with Nile Red after treatment with each drug (Figure 11). It was observed that Tf-PEG-COFs@Pt(IV) reduced fluorescence intensity in tumor cells compared to the CDDP and CDDP-CF groups (p < 0.001), as well as the free conjugate **2** and PEG-COFs@Pt(IV) groups (p < 0.05), indicating its potency in reducing lipid accumulation. Cholesterol serves as a major component of the membrane, and the decreased cholesterol accumulation might influence the integrity of the cell membrane. Herein, membrane integrity was investigated using the membrane stain DiD. As revealed in Figure S13, in the control group, the red fluorescence of DiD diffused laterally to stain the cell membrane, indicating that the membrane was intact. Meanwhile, the red fluorescence in the Tf-PEG-COFs@Pt(IV)-treated group converged in the cytoplasm, further binding with cellular proteins and leading to significantly improved fluorescence intensity compared to the blank group (p < 0.001). These findings indicated that the membrane integrity was disrupted by Tf-PEG-COFs@Pt(IV), which could facilitate cholesterol efflux from cells and further promote the apoptosis of tumor cells.

https://doi.org/10.1021/acs.jmedchem.5c01395
J. Med. Chem. 2025, 68, 20340−20359

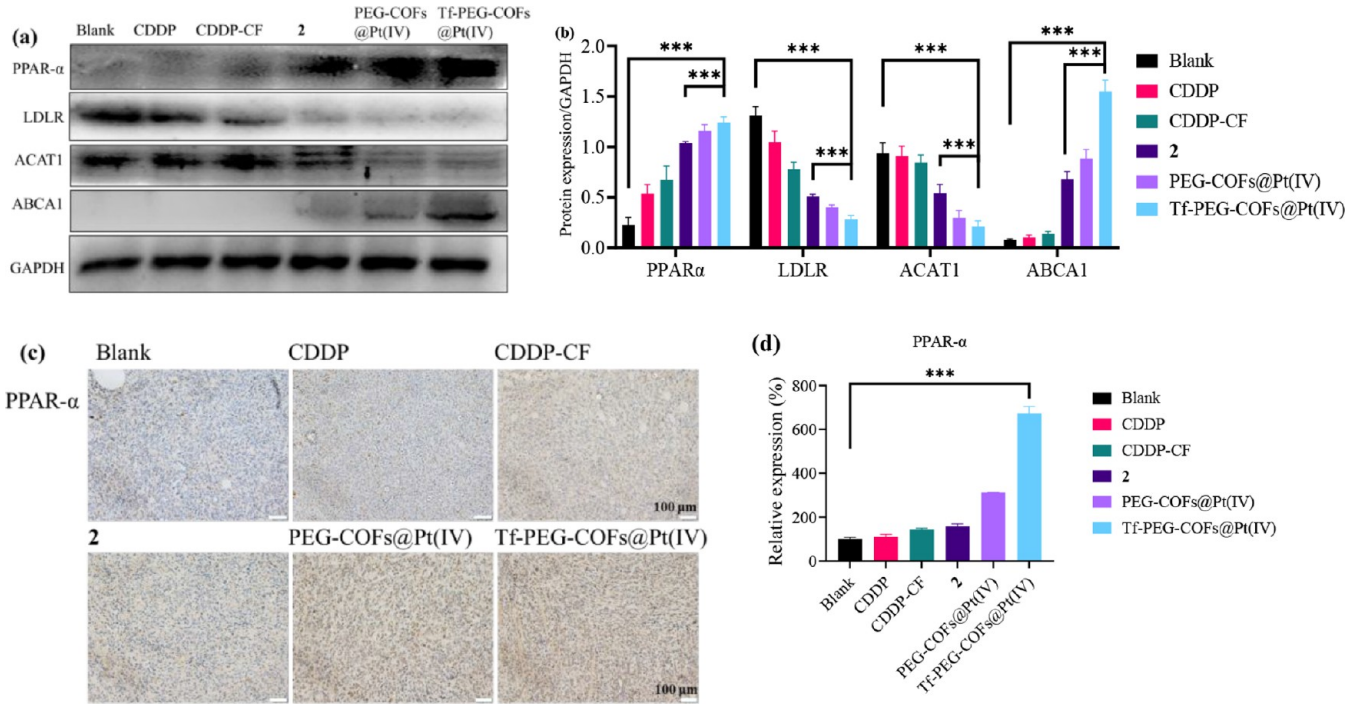

Figure 12. Western blot analysis of PPAR-α, LDLR, ACAT1, and ABCA1 in 4T1 cells treated with and without CDDP (3 μM), CDDP-CF (3 μM/3 μM), compound **2** (3 μM), PEG-COFs@Pt(IV) (3 μM), and Tf-PEG-COFs@Pt(IV) (3 μM) for 24 h at 37 °C. (a) Blots. (b) Relative gray intensity analysis. Relative gray intensity = (gray intensity of indicated protein)/(gray intensity of GAPDH). Immunohistochemical staining (c) and analysis (d) of PPAR-α in 4T1 tumors treated with CDDP, CDDP-CF, compound **2**, PEG-COFs@Pt(IV), and Tf-PEG-COFs@Pt(IV). ***p < 0.001.

To further examine its influence on cholesterol metabolism, we tested the expression of PPAR-α and the proteins low-density lipoprotein receptor (LDLR), acyl-coenzyme A: cholesterol acyltransferase 1 (ACAT1), and ATP-binding cassette subfamily A member 1 (ABCA1), which are responsible for cellular cholesterol uptake, conversion to cholesteryl esters, and the removal of cholesterol from cells. The Western blotting results indicated that Tf-PEG-COFs@Pt(IV) effectively upregulated the expression of PPAR-α (p < 0.001) (Figure 12a,b). Moreover, the promotion of PPAR-α by Tf-PEG-COFs@Pt(IV) was further confirmed immunohistochemically *in vivo* (p < 0.001) (Figure 12c,d). More importantly, Tf-PEG-COFs@Pt(IV) was potent in reducing LDLR and ACAT1 and boosting ABCA1 (p < 0.001), while CDDP exerted negligible influence on these proteins. This trend was similar to that of the Fenofibrate platinum(IV) complexes reported in the literature.[23,24] Notably, the nanodrug Tf-PEG-COFs@Pt(IV) exhibited even more promising potency in regulating these proteins than the free conjugate **2** (p < 0.001), which was probably ascribed to its superior tumor-targeting properties.

Accordingly, Tf-PEG-COFs@Pt(IV) could inhibit cholesterol accumulation in tumor cells by activating PPAR-α, further regulating cholesterol metabolism through a pathway involving LDLR/ACAT1/ABCA1. Modulating cholesterol metabolism in tumor cells opens a new avenue for the exploration of novel platinum-based antitumor agents.

Suppression of EMT Process. Aberrant accumulation of cholesterol increases the risk of EMT in cancer and further promotes tumor metastasis. Regarding the promising potency of Tf-PEG-COFs@Pt(IV) in inhibiting cholesterol accumulation in tumor cells, the proteins *E*-cadherin, *N*-cadherin, Vimentin, and Snail1 involved in EMT were tested by Western blotting and immunohistochemical staining assays in tumor cells and tissues to determine if the potent antitumor activities were associated with EMT reversion.

It was observed in Figure 13 that significant upregulation of *E*-cadherin and downregulation of *N*-cadherin were induced in the Tf-PEG-COFs@Pt(IV) group in comparison with the blank group (p < 0.001). Meanwhile, the proteins Vimentin and Snail1 were also downregulated (p < 0.001). These findings indicated the reversion of the EMT phenotype by Tf-PEG-COFs@Pt(IV) in tumor cells. Furthermore, the immunohistochemical staining results further verified that the EMT process was also inhibited in tumor tissues, with increased *E*-cadherin (p < 0.001) and suppressed *N*-cadherin (p < 0.001) observed in the Tf-PEG-COFs@Pt(IV)-treated tumors compared to the blank group. Suppressed EMT was also noticed in the free complex **2** and nanodrug PEG-COFs@Pt(IV)-treated groups, while CDDP exerted a considerably lower potency. Accordingly, the competence of Tf-PEG-COFs@Pt(IV) in reversing EMT was mainly attributed to active ingredient **2**.

Inhibition of EMT via Regulating PI3K/AKT/mTOR Pathway and Hypoxic TME. Cholesterol accumulation is involved in promoting the PI3K/AKT/mTOR pathway, which is essential for accelerating the EMT process. Herein, the proteins PI3K, *p*-PI3K, AKT, *p*-AKT, mTOR, and *p*-mTOR were evaluated. Results in Figure 14 indicate that PI3K, AKT, and mTOR were all significantly downregulated in 4T1 cells by Tf-PEG-COFs@Pt(IV) compared to the blank group (p < 0.001), while the phosphorylated proteins *p*-PI3K, *p*-AKT, and *p*-mTOR were also suppressed (p < 0.001). Thus, it can be deduced that the PI3K/AKT/mTOR pathway was inhibited in the Tf-PEG-COFs@Pt(IV)-treated cells.

https://doi.org/10.1021/acs.jmedchem.5c01395
J. Med. Chem. 2025, 68, 20340−20359

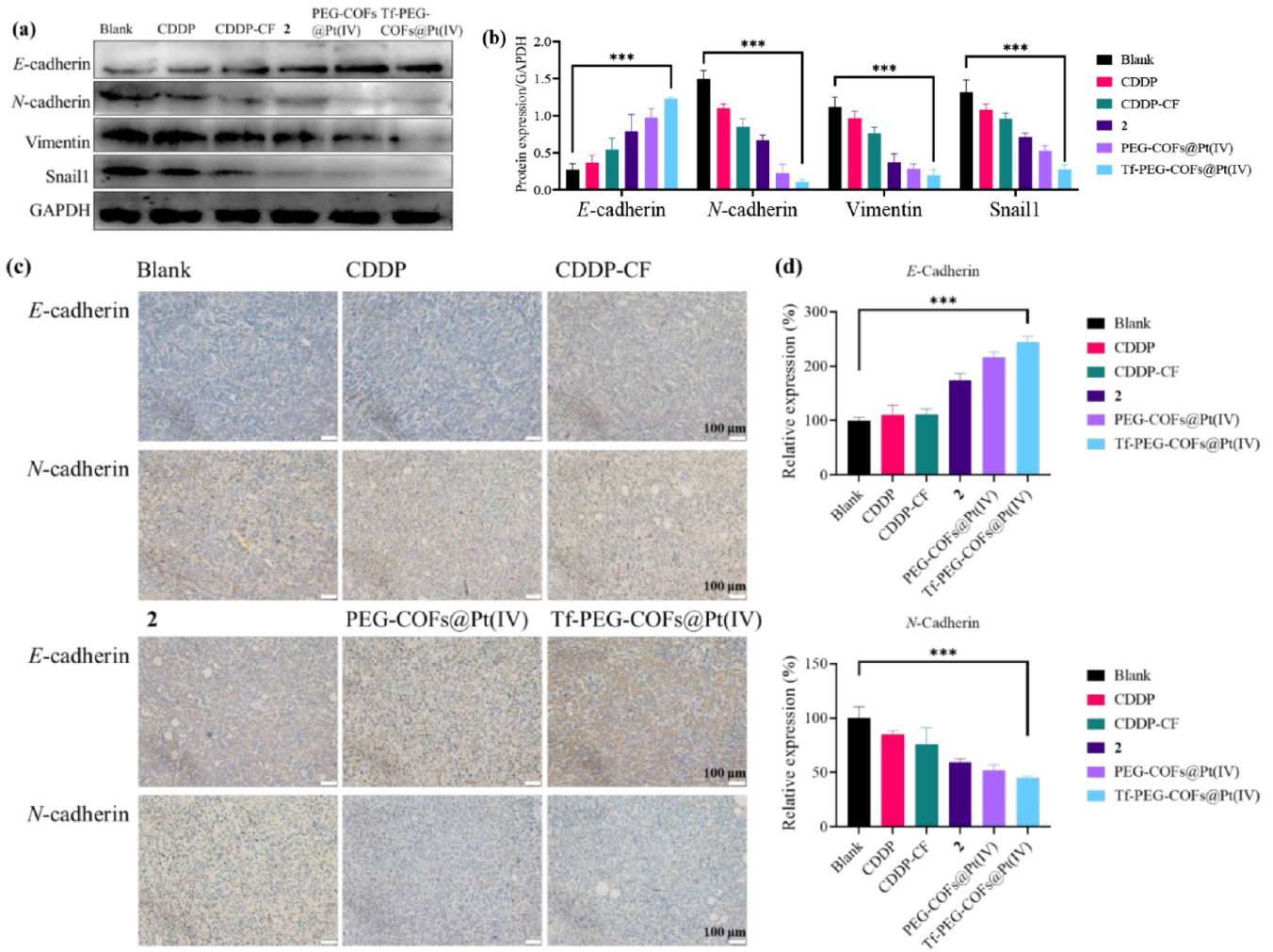

Figure 13. Expression of proteins associated with EMT in tumor cells and tumor tissues. Western blots (a) and analysis (b) for *E*-cadherin, *N*-cadherin, Vimentin, and Snail1 in 4T1 cells incubated with and without CDDP (3 μM), CDDP-CF (3 μM/3 μM), compound **2** (3 μM), PEG-COFs@Pt(IV) (3 μM), and Tf-PEG-COFs@Pt(IV) (3 μM) for 24 h at 37 °C. Immunohistochemical staining (c) and analysis (d) of *E*-cadherin and *N*-cadherin in 4T1 tumors treated with CDDP, CDDP-CF, compound **2**, PEG-COFs@Pt(IV), and Tf-PEG-COFs@Pt(IV). ***$p < 0.001$.

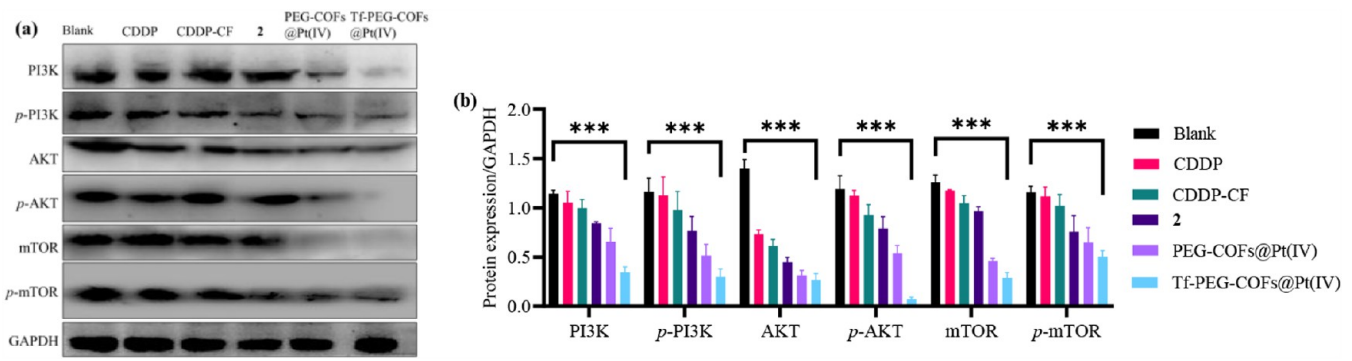

Figure 14. Western blot analysis of PI3K, *p*-PI3K, AKT, *p*-AKT, mTOR, and *p*-mTOR in 4T1 cells treated with and without CDDP (3 μM), CDDP-CF (3 μM/3 μM), compound **2** (3 μM), PEG-COFs@Pt(IV) (3 μM), and Tf-PEG-COFs@Pt(IV) (3 μM) for 24 h at 37 °C. (a) Blots. (b) Relative gray intensity analysis. ***$p < 0.001$.

Furthermore, the hypoxic TME is another factor promoting the progression of EMT. Improved PPAR-α has been proven to be effective in reversing the hypoxic TME by inhibiting the key protein HIF-1α. Reduced hypoxic TME is effective in decreasing angiogenesis in tumors via the HIF-1α/VEGFA axis. It has been widely established that angiogenesis is a pivotal event during tumor invasion and metastasis, as it not only supplies nutrients for tumor growth but also serves as channels for tumor cell metastasis.[41] In this study, the proteins HIF-1α and VEGFA were measured in tumor cells, and CD34, as a marker of angiogenesis, was also tested in tumor tissues.

https://doi.org/10.1021/acs.jmedchem.5c01395
J. Med. Chem. 2025, 68, 20340−20359

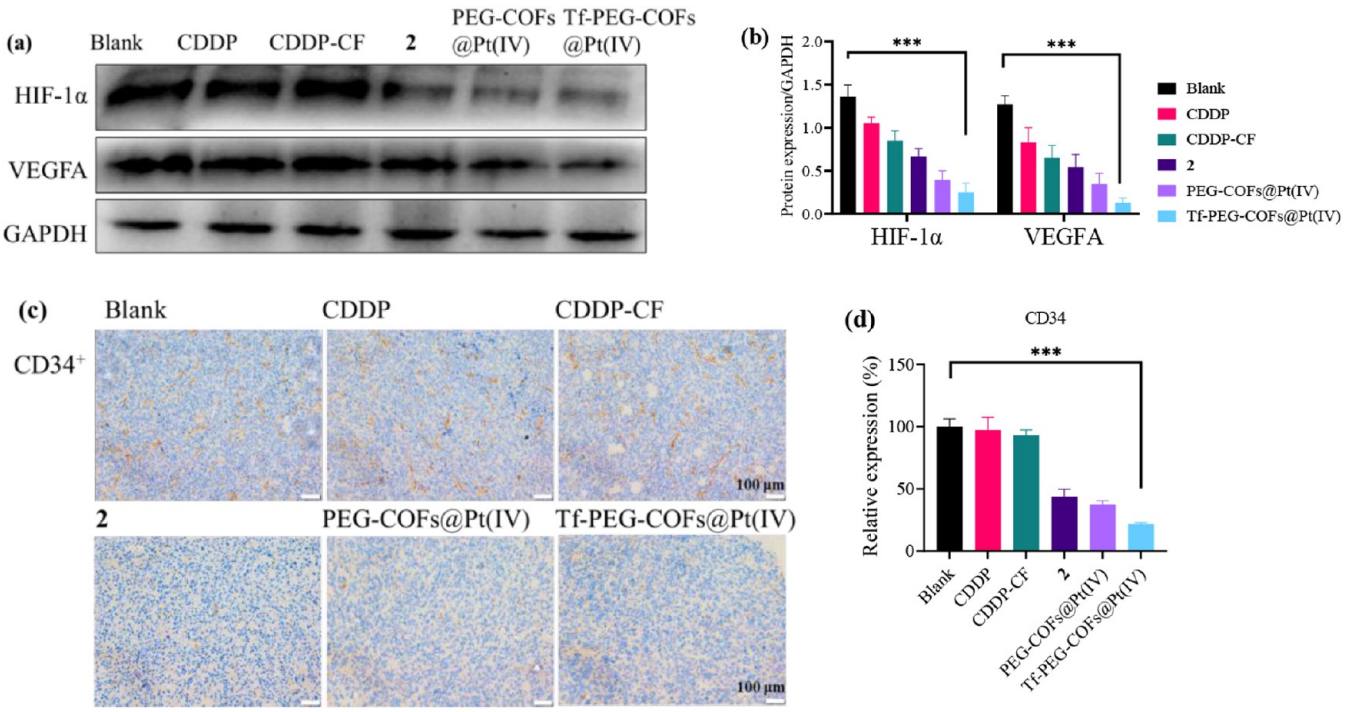

Figure 15. Expression of proteins associated with hypoxic TME in tumor cells and tumor tissues. Western blots (a) and analysis (b) for HIF-α and VEGFA in 4T1 cells incubated with and without CDDP (3 μM), CDDP-CF (3 μM/3 μM), compound **2** (3 μM), PEG-COFs@Pt(IV) (3 μM), and Tf-PEG-COFs@Pt(IV) (3 μM) for 24 h at 37 °C. Immunohistochemical staining (c) and analysis (d) of CD34 in 4T1 tumors treated with CDDP, CDDP-CF, compound **2**, PEG-COFs@Pt(IV), and Tf-PEG-COFs@Pt(IV). ***$p < 0.001$.

As demonstrated in Figure 15a,b, the hypoxia status in tumor cells was ameliorated after treatment with the nanodrug Tf-PEG-COFs@Pt(IV), as evidenced by the decreased expression of HIF-1α ($p < 0.001$). Subsequently, angiogenesis was further inhibited by Tf-PEG-COFs@Pt(IV) through the HIF-1α/VEGFA pathway, and VEGFA expression was suppressed ($p < 0.001$). As a result, the amount of $CD34^+$ blood vessels in tumors treated with Tf-PEG-COFs@Pt(IV) was significantly lower than that in the control group ($p < 0.001$). Meanwhile, CDDP and CDDP-CF exerted a rather negligible influence on angiogenesis (Figure 15c,d). This trend was consistent with the observed antimetastatic activities.

Accordingly, the nanodrug Tf-PEG-COFs@Pt(IV) was effective in inhibiting EMT by suppressing the PI3K/AKT/mTOR and HIF-α/VEGFA cascades, which further synergistically suppressed the metastasis of tumor cells by restraining angiogenesis.

Activation of Antitumor Immunity. The immunosuppressive TME is a hallmark of tumors and plays a significant role in contributing to the failure of chemotherapy. Research has shown that cholesterol accumulation in tumor cells can drive immunosuppression through EMT cascades, while the hypoxic TME also promotes the immune escape of tumor cells. Moreover, abnormal cholesterol metabolism is involved in deactivating tumor-associated macrophages (TAMs) and T-cell immunity. Considering the promising properties of Tf-PEG-COFs@Pt(IV) in promoting cholesterol metabolism and inhibiting EMT and hypoxia, its potential for activating antitumor immunity was further evaluated.

As depicted in Figure 16, the density of $CD3^+$ and $CD8^+$ T cells in tumor tissues significantly increased in the Tf-PEG-COFs@Pt(IV)-treated group compared to the blank group ($p < 0.001$), while a higher number of $CD3^+$ and $CD8^+$ T cells were also observed in the tumors treated with compound **2** and PEG-COFs@Pt(IV) ($p < 0.001$). Then, the polarization of macrophages from the M2 to M1 phenotype was induced by Tf-PEG-COFs@Pt(IV), compound **2**, and PEG-COFs@Pt-(IV), resulting in higher levels of $CD86^+$ M1 tumor-killing TAMs in these groups compared to the blank group, while $CD206^+$ M2 tumor-promoting TAMs were suppressed to lower levels. Notably, the platinum(II) drug CDDP exerted a rather negligible influence on immunity, which is consistent with the literature. Thus, the immunomodulating effects of Tf-PEG-COFs@Pt(IV) were primarily attributed to the CF ligand in active ingredient **2**, rather than the platinum fragment.

Accordingly, the nanodrug Tf-PEG-COFs@Pt(IV) was effective in promoting antitumor immunity by increasing the density of $CD3^+$ and $CD8^+$ T cells, while simultaneously triggering the polarization of macrophages from M2- to M1-type in tumors.

CONCLUSION

Regulating cholesterol metabolism in tumors is a promising approach to modulate EMT progression and further suppress tumor metastasis. CF, as a PPAR-α agonist, is effective in reducing cholesterol accumulation. Herein, a series of new platinum(IV) complexes **1**–**4**, with potential cholesterol-suppressing potency were developed by incorporating CF as a functional ligand into the platinum(IV) system. Furthermore, the nanodrugs PEG-COFs@Pt(IV) and Tf-PEG-COFs@Pt(IV) with COFs as carriers, were prepared. The *in vitro* antitumor activities revealed that both the ligand and the platinum core significantly influenced the antitumor outcomes of the CF platinum(IV) conjugates. Notably, the CDDP-derived conjugate **2** with a mono CF ligand exhibited the most promising efficacy, with IC_{50} values lower than 1.44 μM, which

https://doi.org/10.1021/acs.jmedchem.5c01395
J. Med. Chem. 2025, 68, 20340−20359

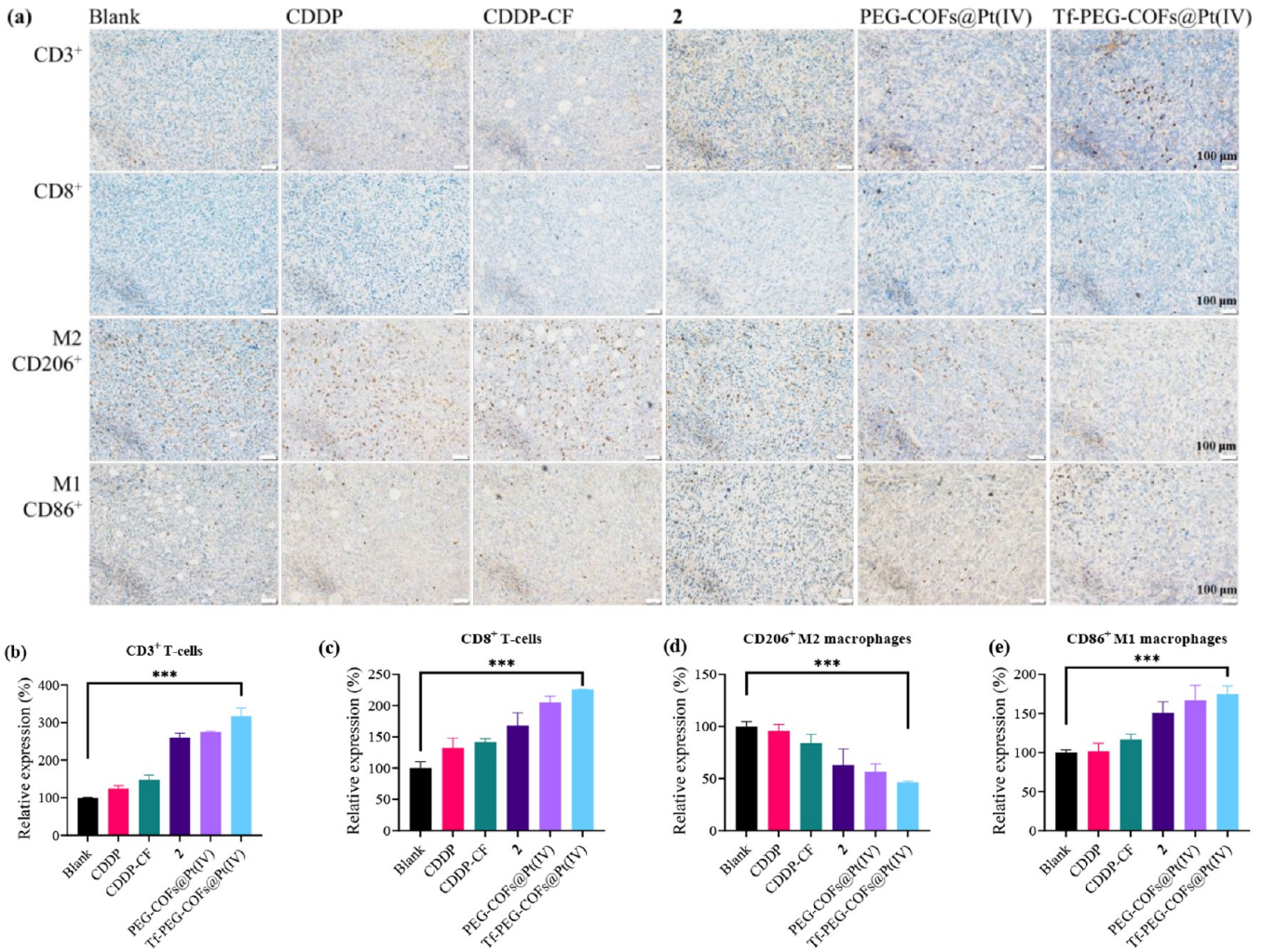

Figure 16. Immunohistochemical staining of TILs and TAMs in tumor tissues in the antitumor growth assay *in vivo*. (a) Immunohistochemical staining images of 4T1 tumors treated with CDDP, CDDP-CF, compound **2**, PEG-COFs@Pt(IV), and Tf-PEG-COFs@Pt(IV). (b–e) Quantified data of $CD3^+$and $CD8^+$ T-cells, and $CD206^+$ M2 and $CD86^+$ M1 macrophages. ***$p < 0.001$.

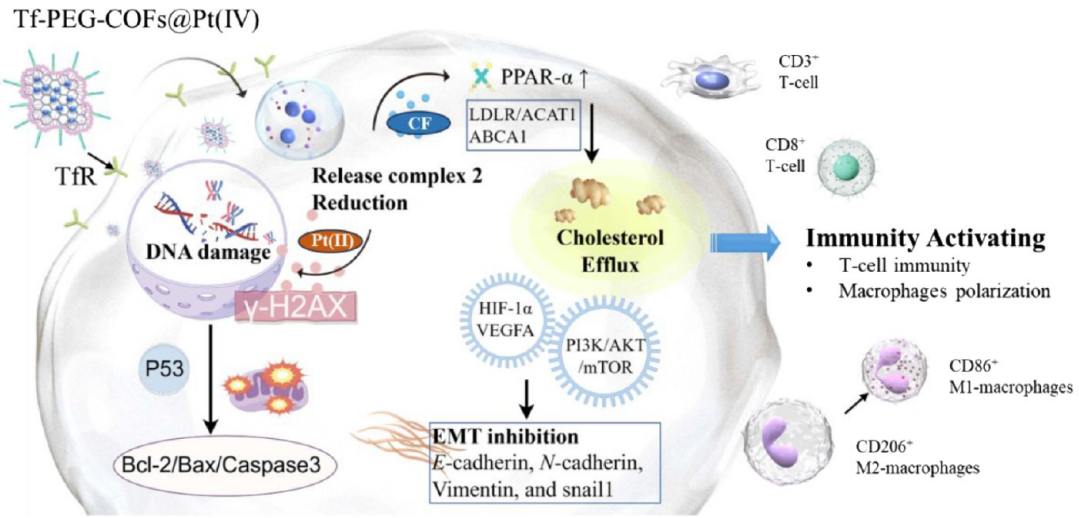

Figure 17. Proposed mechanism of nanodrug Tf-PEG-COFs@Pt(IV) in tumor cells.

were even more potent than the reference drugs CDDP and OXP. Subsequently, the preparation of the nanodrug Tf-PEG-COFs@Pt(IV) further elevated the antitumor activities to 0.05–0.19 μM. Moreover, Tf-PEG-COFs@Pt(IV) exhibited high potency in overcoming drug resistance to CDDP and reducing toxicities. Subsequently, Tf-PEG-COFs@Pt(IV) demonstrated promising antitumor activities against 4T1 tumors *in vivo*, leading to a dramatically higher TGI of

https://doi.org/10.1021/acs.jmedchem.5c01395
J. Med. Chem. 2025, 68, 20340–20359

77.3% compared to the reference drug CDDP and the mixture CDDP-CF (TGI = 18.6% and 27.1%, $p < 0.001$). Additionally, it showed significant efficacy in reducing the toxicities associated with the active ingredient **2** and significantly prolonged the survival period of mice. More importantly, Tf-PEG-COFs@Pt(IV) exhibited significant antimetastatic activities *in vivo*, reducing the number of nodules in lung tissues to 15.0% of the blank group in pulmonary metastasis models, which was much lower than PEG-COFs@Pt(IV) (22.3%, $p < 0.05$), complex **2** (27.5%, $p < 0.001$), and the reference drugs CDDP (53.5%, $p < 0.001$) and CDDP-CF (52.0%, $p < 0.001$). The mechanism investigation revealed that the Tf ligand endowed the nanodrug Tf-PEG-COFs@Pt(IV) with high tumor-targeting properties, allowing it to reach tumor sites at a higher level than PEG-COFs@Pt(IV) and free conjugate **2** ($p < 0.001$). Tf-PEG-COFs@Pt(IV) could then gradually release active ingredient **2** in a sustained manner. Complex **2** was reduced to its divalent form in the reducing TME and caused significant DNA damage through the platinum core, as indicated by the upregulation of γ-H2AX and p53 (Figure 17). Subsequently, notable mitochondria-mediated apoptosis was initiated via the Bcl-2/Bax/caspase-3 pathway, accompanied by the induction of $\Delta\Psi_m$ collapse. Moreover, cholesterol accumulation was inhibited by the CF ligand through the promotion of PPAR-α expression, which further regulated the LDLR/ACAT1/ABCA1 signaling pathway involved in cholesterol metabolism. Subsequently, the EMT process was remarkably reversed by regulating the PI3K/AKT/mTOR pathway and modulating the hypoxic TME. Additionally, antitumor immunity was stimulated by Tf-PEG-COFs@Pt(IV) through increasing the density of $CD3^+$ and $CD8^+$ T cells and simultaneously triggering the polarization of macrophages from M2- to M1-type in tumors. Eventually, a nanodrug, Tf-PEG-COFs@Pt(IV) based on a CF platinum(IV) hybrid with excellent antiproliferative and antimetastatic properties, was developed in this work, which is crucial for future efforts in the development of new antimetastatic agents.

EXPERIMENTAL SECTION

General. The platinum(II) drugs CDDP and OXP were obtained from Boyuan Pharmaceutical Co., Ltd., (Jinan, China). Other chemicals were obtained from suppliers including Sigma, J&K, Aladdin, Macklin, and Innochem, and were utilized without further purification unless otherwise specified. Reactions were conducted under a nitrogen atmosphere in flame-dried glassware with magnetic stirring. Nuclear magnetic resonance (NMR) spectra were acquired using a Bruker spectrometer operating at 500 MHz for ^{1}H NMR and 126 MHz for ^{13}C NMR. Mass spectrometry (MS) analyses were performed using a Shimadzu LC-MS/MS 8040 mass spectrometer with electrospray ionization (ESI). High-resolution mass spectrometry (HRMS) data were collected by using a Waters G2-XS QToF mass spectrometer. Atomic absorption spectroscopy (AAS) was conducted with a Shimadzu AA-6880 instrument. Flow cytometric analyses were performed on a Millipore Guava easyCyte 8HT flow cytometer. High-performance liquid chromatography (HPLC) analyses were carried out on either a Thermo Ultimate 3000 RS or a Shimadzu LC-20A system. All compounds were >95% pure, as determined by HPLC analysis.

Synthetic Procedure. *Preparation of Oxoplatins O1 and O2 (details provided in ESI). Synthesis of Compound 1.* The CF (145 mg, 0.50 mmol) and TBTU (160 mg, 0.50 mmol) were dissolved in 5 mL of anhydrous DMF and stirred at room temperature for 15 min. Subsequently, TEA (70 μL, 0.50 mmol) was added to the solution, and stirring was continued for an additional 15 min. Oxoplatin **O1** (100 mg, 0.30 mmol) was then incorporated into the reaction mixture, which was maintained at 50 °C for 48 h under a nitrogen atmosphere in the dark. After the reaction was completed, the solvent was evaporated under reduced pressure. The resulting crude product was purified via silica gel column chromatography, yielding compound **1** as a pale solid (150.9 mg, 57.7%). The purity of the compound was 95.2% determined by HPLC analysis using a MeOH/H_2O (80/20) solvent system. ^{1}H NMR (500 MHz, DMSO-d_6) δ: 7.13−7.12 (m, J = 8.7 Hz, 4H), 6.90−6.88 (m, J = 8.7 Hz, 4H), 6.58 (s, 6H), 3.03−2.99 (t, J = 9.7 Hz, 2H), 2.06−2.01 (m, J = 10.4 Hz, 4H), 1.47 (s, 12H). ^{13}C NMR (126 MHz, DMSO-d_6) δ: 180.9, 154.7, 129.2, 126.8, 118.6, 79.1, 61.9, 33.8, 25.9, 25.6, 24.7. HRMS: calcd for $[M + Na]^+$: 895.9937 (M = $C_{26}H_{32}Cl_6N_2O_6Pt$); found: 895.9935.

Synthesis of Compound 2. The CF (95 mg, 0.33 mmol) and TBTU (59 mg, 0.33 mmol) were dissolved in 5 mL of anhydrous DMF and stirred at room temperature for 15 min. Subsequently, TEA (46 μL, 0.33 mmol) was added to the solution, and the stirring was continued for an additional 15 min. Oxoplatin **O1** (100 mg, 0.30 mmol) was then incorporated into the reaction mixture, which was maintained at 50 °C for 48 h under a nitrogen atmosphere in the dark. After the reaction was completed, the solvent was evaporated under reduced pressure. The resulting crude product was purified via silica gel column chromatography, yielding compound **2** as a pale solid (41.9 mg, 23.2%). The purity of the compound was determined to be 97.6% by HPLC analysis using a MeOH/H_2O (85/15) solvent system. ^{1}H NMR (500 MHz, DMSO-d_6) δ 7.18−7.07 (m, 2H), 6.89−6.77 (m, 2H), 6.20−5.82 (m, 6H), 2.99 (t, J = 9.7 Hz, 1H), 2.04−1.99 (m, 2H), 1.44 (s, 6H). ^{13}C NMR (126 MHz, DMSO-d_6) δ: 180.8, 155.0, 129.1, 126.3, 118.3, 79.6, 61.9, 33.9, 25.9, 25.6, 24.7. HRMS: calcd for $[M + Na]^+$: 625.9717 (M = $C_{13}H_{20}Cl_4N_2O_4Pt$), found: 625.9716.

Synthesis of Compound 3. The CF (167 mg, 0.58 mmol) and TBTU (186 mg, 0.58 mmol) were dissolved in 5 mL of anhydrous DMF and subjected to stirring at room temperature for 15 min. Subsequently, TEA (80 μL, 0.58 mmol) was introduced into the solution, and the stirring was continued for an additional 15 min. Oxoplatin **O2** (100 mg, 0.23 mmol) was then incorporated into the reaction mixture, which was maintained at 50 °C for 48 h under a nitrogen atmosphere and in the absence of light. After the reaction was completed, the solvent was evaporated under reduced pressure. The resulting crude product was purified via silica gel column chromatography, yielding compound **3** as a pale solid (118.5 mg, 53.1%). The purity of the compound was determined to be 97.2% by HPLC analysis using a MeOH/H_2O (85/15) solvent system. ^{1}H NMR (500 MHz, Methanol-d_4) δ: 7.14 (d, J = 8.7 Hz, 4H), 6.79 (d, J = 7.1 Hz, 4H), 2.94−2.85 (m, 2H), 2.59−2.50 (m, 2H), 2.25−2.14 (m, 2H), 1.97−1.93 (m, 2H), 1.90−1.86 (m, 2H), 1.65−1.59 (m, 2H), 1.58 (s, 12H), 1.46−1.39 (m, 2H), 1.21−1.97 (m, 2H). ^{13}C NMR (126 MHz, Methanol-d_4) δ: 184.1, 166.4, 156.4, 156.3, 130.9, 130.8, 129.4, 129.3, 119.3, 119.2, 81.3, 81.2, 63.4, 63.3, 62.4, 35.9, 32.7, 26.4, 26.3, 25.0. HRMS: calcd for $[M + Na]^+$: 994.0977 (M = $C_{34}H_{40}Cl_4N_2O_{10}Pt$), found: 994.0974.

https://doi.org/10.1021/acs.jmedchem.5c01395
J. Med. Chem. 2025, 68, 20340−20359

Synthesis of Compound ***4****.* The CF (74 mg, 0.25 mmol) and TBTU (82 mg, 0.25 mmol) were dissolved in 5 mL of anhydrous DMF and subjected to stirring at room temperature for 15 min. Subsequently, TEA (35 μL, 0.25 mmol) was introduced into the solution, and the stirring was continued for an additional 15 min. Oxoplatin **O2** (100 mg, 0.23 mmol) was then incorporated into the reaction mixture, which was maintained at 50 °C for 48 h under a nitrogen atmosphere and in the absence of light. After the reaction was completed, the solvent was evaporated under reduced pressure. The resulting crude product was purified via silica gel column chromatography, yielding compound **4** as a pale solid (50.6 mg, 31.4%). The purity of the compound was determined to be 97.5% by HPLC analysis using a MeOH/H_2O (85/15) solvent system. ^{1}H NMR (500 MHz, Methanol-d_4) δ: 7.14 (d, J = 8.7 Hz, 2H), 6.79 (d, J = 6.6 Hz, 2H), 2.93−2.84 (m, 1H), 2.80 − 2.69 (m, 1H), 2.57 (m, J = 4.4 Hz, 1H), 2.27−2.15 (m, 2H), 1.98−1.82 (m, 2H), 1.63 (m, J = 11.3 Hz, 2H), 1.56 (m, 1H), 1.54−1.49 (m, 6H), 1.47−1.33 (m, 1H), 1.27−1.11 (m, 2H). ^{13}C NMR (126 MHz, Methanol-d_4) δ: 184.9, 166.8, 156.6, 130.8, 129.1, 119.2, 81.5, 63.8, 62.4, 61.9, 36.0, 32.6, 26.2, 25.2, 9.3. HRMS: calcd for $[M + Na]^+$: 724.0768 (M = $C_{21}H_{28}Cl_2N_2O_8Pt$), found: 724.0769.

Preparation of Nanoparticles COFs@Pt(IV), PEG-COFs@Pt(IV) and Tf-PEG-COFs@Pt(IV). The COFs were dispersed in 0.5 mL of DMF, and the suspension was ultrasonicated for 1 h. Then, complex **2** (**2**:COFs = 1:1, w/w) in 0.5 mL of DMF was added to the suspension dropwise over 20 min under stirring. Subsequently, distilled water (9 mL) was added to the mixture dropwise over 20 min under stirring, followed by further stirring for an additional 30 min. The resultant nanoparticles COFs@Pt(IV) were obtained.

Subsequently, the solution of COFs@Pt(IV) was freeze-dried to remove the solvent. The particles were suspended in dioxane (0.5 mL), and DSPE-PEG_{2000} (**2**: DSPE-PEG_{2000} = 3:1, mol/mol) was added. The mixture was slowly dropped into water (20 mL) over 20 min under stirring, and the resultant mixture was further stirred for another 30 min. The obtained nanoparticles were homogenized by a D-3L homogenizer (PhD, USA) under optimal homogenization conditions of 100 MPa for 60 min to reduce the size. The solution was dialyzed (MWCO = 8−14 kDa) twice against deionized water to remove the organic solvent. Afterward, the solution was collected, and PEG-COFs@Pt(IV) was obtained. The encapsulation efficiency of complex **2** in PEG-COFs@Pt(IV) was 86.4%, as determined by AAS. The amount of active ingredient platinum(IV) complex **2** in the nanodrugs was determined by measuring the Pt content in the nanodrugs using an AAS assay, which was applied in the subsequent biological experiments.

The tumor-targeting nanodrug Tf-PEG-COFs@Pt(IV) was obtained by modifying PEG-COFs@Pt(IV) with Tf-modified DSPE-PEG_{2000}-Tf. Briefly, DSPE-PEG_{2000}-Tf was added to a solution of nanoparticles PEG-COFs@Pt(IV) at a ratio of 3:4 (DSPE-PEG_{2000}-Tf/DSPE-PEG_{2000}, mol/mol). The mixture was incubated at 30 °C for 1 h under stirring, resulting in the formation of Tf-PEG-COFs@Pt(IV). Subsequently, the binding ratio of Tf to PEG-COFs@Pt(IV) was 82.6%, as determined using a BCA kit (Beyotime Biotechnology, China).

The particle size distribution of all nanoparticles was measured by DLS, and the morphology of the nanoparticles was imaged by SEM.

Preparation of DiD-Labled Nanoparticles DiD-PEG-COFs@Pt(IV) and DiD-Tf-PEG-COFs@Pt(IV). The DiD was encapsulated in the nanoparticles along with Complex **2**. Complex **2** and DiD (1% of DSPE-PEG_{2000}, w/w) were dissolved in 0.5 mL of DMF, which were then added to the suspension of COFs in 0.5 mL of DMF. Subsequently, the mixture was dropped into water (9 mL), and the resultant solution was stirred for 30 min. The DiD-labeled Pt(IV), was obtained. Following this, the nanodrugs DiD-PEG-COFs@Pt(IV) and DiD-Tf-PEG-COFs@Pt(IV) were prepared according to the procedures described for PEG-COFs@Pt(IV) and Tf-PEG-COFs@Pt(IV).

Stability of Nanoparticles PEG-COFs@Pt(IV) and Tf-PEG-COFs@Pt(IV). The nanoparticles PEG-COFs@Pt(IV) and Tf-PEG-COFs@Pt(IV) were stored at 4 °C for 7 days. The particle size was monitored by DLS to detect their storage stability. The experiments were conducted in triplicate.

Cell Culture. Cell lines, including human lung cancer (A549), CDDP-resistant human lung cancer (A549R), murine breast cancer (4T1), human liver cancer (HepG2), and a human normal liver cell line (LO2), were evaluated in this study for the antitumor activities of CF platinum(IV) conjugates and the nanodrugs, with CF, CDDP-CF, CDDP, and OXP as reference drugs. These cell lines were originally obtained from the American Type Culture Collection (ATCC) or Pricella Biotechnology Co., Ltd. (Wuhan, China), and were maintained in the laboratory. The HepG2 cells were cultured in Dulbecco's Modified Eagle Medium (DMEM), while the A549, A549R, LO2, and 4T1 cells were cultured in RPMI 1640 medium. Both media were supplemented with 10% fetal bovine serum (FBS) and 1% penicillin−streptomycin, and the cells were maintained in a humidified atmosphere. All culture reagents were purchased from Solarbio (Beijing, China).

Animals. The antitumor properties of CF platinum(IV) complexes and nanodrugs were assessed using female BALB/c mice (18−20 g) as the experimental model. These mice were purchased from Pengyue Experimental Animal Company (Jinan, China) and were maintained under standardized conditions (12 h light/dark cycle, 23 ± 2 °C) with free access to food and water. All experimental procedures strictly adhered to the guidelines for the care and use of laboratory animals (NIH Publication 8023, revised 1978). The experiments were approved by the Institutional Animal Ethics Committee of Liaocheng University (No. AP2024022955).

Antitumor Growth Assay *In Vivo*. The antitumor efficacy was assessed in BALB/c mice bearing 4T1 tumors. Tumor cells (1×10^6 in 0.15 mL PBS) were injected subcutaneously into the left flanks of the mice. When the tumors became palpable on day 3, the mice were randomly divided into six groups (n = 5): blank, free complex **2**, nanoparticles PEG-COFs@Pt(IV), Tf-PEG-COFs@Pt(IV), CDDP, and CDDP-CF. Complex **2** and CDDP were administered in a saline solution containing 5% N,N-dimethylformamide (DMF), while the control group received the vehicle alone. Nanoparticles were administered directly after preparation. All agents were injected (i.p.) at a dosage of 2 mg of Pt/kg on days 3, 6, and 9. Tumor volume was calculated using the formula $V = W^2 \times L/2$, where W was the tumor width and L was the tumor length. Body weight was monitored throughout the experiment. On day 12, the mice were euthanized, and blood, tumors, and major organs (heart, liver, spleen, lung, and kidney) were collected. Tumor growth inhibition (TGI) was determined using the formula: TGI (%)

https://doi.org/10.1021/acs.jmedchem.5c01395
J. Med. Chem. 2025, 68, 20340−20359

= (1 − tumor weight of the drug-treated group/tumor weight of the control group) × 100%.

Survival Analysis *In Vivo*. Differences in survival *in vivo* studies were determined based on Kaplan−Meier survival analysis. The establishment of female BALB/c mice bearing 4T1 tumors was conducted as previously described. Upon tumors becoming palpable on day 3, the mice were randomly divided into six groups (n = 10): blank, free complex **2**, nanoparticles PEG-COFs@Pt(IV), Tf-PEG-COFs@Pt(IV), CDDP, and CDDP-CF. Each treatment was administered intraperitoneally at a dosage of 2 mg of Pt/kg on days 3, 6, and 9. Subsequently, the mice were monitored until day 28. Mice were removed from the study under the following conditions: (i) a loss of 20% of initial body weight, (ii) tumors reaching 20 mm in diameter, or (iii) mortality. The survival of the mice was systematically recorded, and the Kaplan−Meier survival curve was drawn after the experiment.

Antimetastatic Assay *In Vivo*. The antimetastatic activities were evaluated in female BALB/c mice. Pulmonary metastasis models were established through the injection of 4T1 cells (1×10^5 in 0.2 mL PBS) via the tail vein. The mice were randomly assigned to six groups (n = 5): blank, free complex **2**, nanoparticles PEG-COFs@Pt(IV), Tf-PEG-COFs@Pt(IV), CDDP, and CDDP-CF. Complex **2** and CDDP were administered in a saline solution containing 5% DMF, while the control group received the vehicle alone. Nanoparticles were administered directly after preparation. All agents were injected (i.p.) at a dosage of 2 mg Pt/kg on days 3, 6, and 9. On day 12, the mice were euthanized, and lung tissues were collected and fixed in Bouin's fluid. The number of visible metastatic nodules on the lung surface was counted, and the inhibition rate in comparison with the blank group was calculated. Additionally, nodules within the lung tissue were examined using H&E staining assay.

Tumor-Targeting Investigations *In Vivo*. The fluorescent probe DiD, with far-red fluorescence, was employed to assess the biodistribution of the nanoparticles *in vivo*. Female BALB/c mice with murine 4T1 tumors were used in the tumor-targeting studies. Tumor cells (1×10^6 in 0.15 mL of PBS) were subcutaneously injected into the left flanks of the mice. When tumors reached 200−300 mm^3 on day 7, the mice were randomly assigned to three groups (n = 3): the mixture of DiD with complex **2** (DiD-**2**), DiD-labeled nanoparticles (DiD-PEG-COFs and DiD-Tf-PEG-COFs@Pt(IV). Each group received an equivalent volume of drugs (2 mg of Pt/kg) with the same DiD concentration intravenously (i.v.). The mice were briefly anesthetized using isoflurane inhalation and subsequently scanned at 1, 2, 4, 8, 12, and 24 h using an imaging system (Alliance 4.7, UVITEC, Cambridge, UK). Afterward, the mice were euthanized, and tissues, including the tumor, heart, liver, spleen, lung, and kidney, were harvested and imaged. The fluorescence intensity was quantified to evaluate the distribution and tumor-targeting efficacy of the drugs *in vivo*.

■ ASSOCIATED CONTENT

Supporting Information

The Supporting Information is available free of charge at https://pubs.acs.org/doi/10.1021/acs.jmedchem.5c01395.

Synthetic procedure; stability of nanoparticles; antitumor activities *in vivo*; antimetastatic activities *in vitro*; tumor-targeting properties; DNA damage properties; induction of mitochondria-mediated apoptosis; inhibition of cholesterol accumulation; experimental section; ^{1}H NMR, ^{13}C NMR, MS, HRMS, and HPLC spectra of CF platinum(IV) complexes (PDF)

Molecular formula strings (CSV)

■ AUTHOR INFORMATION

Corresponding Authors

Shilei Ji − *Institute of Biopharmaceutical Research, State Key Laboratory of Macromolecular Drugs and Large-scale Preparation, Shandong Provincial Key Laboratory of Applied Technology for Protein and Peptide Drugs, Liaocheng University, Liaocheng 252059, P. R. China*; Email: jishileihy@163.com

Qingpeng Wang − *Institute of Biopharmaceutical Research, State Key Laboratory of Macromolecular Drugs and Large-scale Preparation, Shandong Provincial Key Laboratory of Applied Technology for Protein and Peptide Drugs, Liaocheng University, Liaocheng 252059, P. R. China*; orcid.org/0000-0002-2093-8237; Email: lywqp@126.com

Authors

Shuaiqi Feng − *Institute of Biopharmaceutical Research, State Key Laboratory of Macromolecular Drugs and Large-scale Preparation, Shandong Provincial Key Laboratory of Applied Technology for Protein and Peptide Drugs, Liaocheng University, Liaocheng 252059, P. R. China*

Yan Chen − *Institute of Biopharmaceutical Research, State Key Laboratory of Macromolecular Drugs and Large-scale Preparation, Shandong Provincial Key Laboratory of Applied Technology for Protein and Peptide Drugs, Liaocheng University, Liaocheng 252059, P. R. China; Key Laboratory of Functional Molecular Engineering of Guangdong Province, School of Chemistry and Chemical Engineering, South China University of Technology, Guangzhou 510640, China*

Zhifang Liu − *Institute of Biopharmaceutical Research, State Key Laboratory of Macromolecular Drugs and Large-scale Preparation, Shandong Provincial Key Laboratory of Applied Technology for Protein and Peptide Drugs, Liaocheng University, Liaocheng 252059, P. R. China*

Complete contact information is available at: https://pubs.acs.org/10.1021/acs.jmedchem.5c01395

Notes

The authors declare no competing financial interest.

■ ACKNOWLEDGMENTS

This work was supported by the Youth Innovation Technology Project of Higher School in Shandong Province (No. 2021KJ099), the National Natural Science Foundation of China (No. 21807056), and the Natural Science Foundation of Shandong Province (No. ZR2020KH005). This work was also technically supported by the Shandong Collaborative Innovation Center for Antibody Drugs, the Engineering Research Center for Nanomedicine and Drug Delivery Systems, and the Taishan Scholar Research Group. We thank Home for Researchers, and some figures were drawn using Figdraw.

■ ABBREVIATIONS

AAS	atomic absorption spectrometry
AsA	ascorbic acid
CBP	carboplatin

CDDP	cisplatin
CF	ciprofibrate
COFs	covalent organic frameworks
DCFH-DA	2′,7′-dichlorofluorescein diacetate
DLS	dynamic laser light scattering
DMF	*N,N*-dimethylformamide
DMSO	dimethyl sulfoxide
EMT	epithelial-mesenchymal transition
5′-GMP	guanosine-5′-monophosphate
H&E	hematoxylin-eosin
HPLC	high-performance liquid chromatography
IC_{50}	half-maximal inhibitory concentration
i.p.	intraperitoneal injection
i.v.	intravenous injection
MTT	(3-(4,5-dimethylthiazol-2-yl)-2,5-diphenyltetrazolium bromide
NDDS	nanodrug delivery systems
OXP	oxaliplatin
PI	propidium iodide
PPAR	peroxisome proliferator-activated receptor
RF	resistant factor
SI	selective index
TBTU	N,N,N′,N′-tetramethyl-O-(benzotriazol-1-yl)-uronium tetrafluoroborate
TEA	N,N,N-triethylamine; Tf: transferrin
TGI	tumor growth inhibition
TILs	tumor-infiltrating lymphocytes
TME	tumor microenvironment

REFERENCES

(1) Kiri, S.; Ryba, T. Cancer, metastasis, and the epigenome. *Mol. Cancer* **2024**, *23* (1), 154.

(2) Hill, W.; Weeden, C. E.; Swanton, C. Tumor promoters and opportunities for molecular cancer prevention. *Cancer Discovery* **2024**, *14* (7), 1154−1160.

(3) Zhang, C.; Xu, C.; Gao, X.; Yao, Q. Platinum-based drugs for cancer therapy and anti-tumor strategies. *Theranostics* **2022**, *12* (5), 2115−2132.

(4) Li, S.; Chen, Y.; Feng, S.; Liu, Z.; Gan, L.; Wang, Q. Autophagy-targeted Pt(IV) agents: a new horizon in antitumor drug development. *Dalton Trans.* **2025**, *54* (5), 1770−1778.

(5) Ravera, M.; Gabano, E.; McGlinchey, M. J.; Osella, D. Pt (IV) antitumor prodrugs: dogmas, paradigms, and realities. *Dalton Trans.* **2022**, *51* (6), 2121−2134.

(6) Wang, M.; Li, G.; Jiang, G.; Cai, J.; Liu, Z.; Huang, R.; Huang, X.; Wang, H. Novel NF-κB inhibitor-conjugated Pt(IV) prodrug to enable cancer therapy through ROS/ER stress and mitochondrial dysfunction and overcome multidrug resistance. *J. Med. Chem.* **2024**, *67* (8), 6218−6237.

(7) Zhong, Y.; Jia, C.; Zhang, X.; Liao, X.; Yang, B.; Cong, Y.; Pu, S.; Gao, C. Targeting drug delivery system for platinum(IV)-Based antitumor complexes. *Eur. J. Med. Chem.* **2020**, *194*, 112229.

(8) De Visser, K. E.; Joyce, J. A. The evolving tumor microenvironment: From cancer initiation to metastatic outgrowth. *Cancer Cell* **2023**, *41* (3), 374−403.

(9) Chen, Y.; Zhang, M.; He, Y.; Li, S.; Feng, S.; Liu, Z.; Zhang, N.; Liu, M.; Wang, Q. Canadine platinum(IV) complexes targeting epithelial-mesenchymal transition as antiproliferative and antimetastatic agents. *J. Med. Chem.* **2024**, *67* (15), 12868−12886.

(10) Zhang, M.; Chen, Y.; Liu, Z.; Liu, M.; Wang, Q. Series of desloratadine platinum(IV) hybrids displaying potent antimetastatic competence by inhibiting epithelial-mesenchymal transition and arousing immune response. *J. Med. Chem.* **2024**, *67* (3), 2031−2048.

(11) Zhang, F.; Du, G. Dysregulated lipid metabolism in cancer. *World J. Biol. Chem.* **2012**, *3* (8), 167−174.

(12) Xiao, M.; Xu, J.; Wang, W.; Zhang, B.; Liu, J.; Li, J.; Xu, H.; Zhao, Y.; Yu, X.; Shi, S. Functional significance of cholesterol metabolism in cancer: from threat to treatment. *Exp. Mol. Med.* **2023**, *55* (9), 1982−1995.

(13) Jiang, W.; Jin, W. L.; Xu, A. M. Cholesterol metabolism in tumor microenvironment: cancer hallmarks and therapeutic opportunities. *Int. J. Biol. Sci.* **2024**, *20* (6), 2044−2071.

(14) Yan, A.; Jia, Z.; Qiao, C.; Wang, M.; Ding, X. Cholesterol metabolism in drugresistant cancer (Review). *Int. J. Oncol.* **2020**, *57* (5), 1103−1115.

(15) Luo, J.; Yang, H.; Song, B. L. Mechanisms and regulation of cholesterol homeostasis. *Nat. Rev. Mol. Cell Biol.* **2020**, *21*, 225−245.

(16) Nafees, M.; He, F.; Feng, L.; Hanif, M.; Yang, P. Harnessing metal complexes to target tumour bioenergetics and metabolic vulnerabilities. *Inorg. Chem. Front.* **2025**, *12*, 4151.

(17) Zhang, K. L.; Zhu, W. W.; Wang, S. H.; Gao, C.; Pan, J. J.; Du, Z. G.; Lu, L.; Jia, H. L.; Dong, Q. Z.; Chen, J. H.; Lu, M.; Qin, L. X. Organ-specific cholesterol metabolic aberration fuels liver metastasis of colorectal cancer. *Theranostics* **2021**, *11* (13), 6560−6572.

(18) Jiang, S.; Wang, X.; Song, D.; Liu, X.; Gu, Y.; Xu, Z.; Wang, X.; Zhang, X.; Ye, Q.; Tong, Z.; Yan, B.; Yu, J.; Chen, Y.; Sun, M.; Wang, Y.; Gao, S. Cholesterol induces epithelial-to-mesenchymal transition of prostate cancer cells by suppressing degradation of EGFR through APMAP. *Cancer Res.* **2019**, *79* (12), 3063−3075.

(19) Brindisi, M.; Frattaruolo, L.; Fiorillo, M.; Dolce, V.; Sotgia, F.; Lisanti, M. P.; Cappello, A. R. New insights into cholesterol-mediated ERRα activation in breast cancer progression and pro-tumoral microenvironment orchestration. *FEBS J.* **2023**, *290* (6), 1481−1501.

(20) Jin, H.; He, Y.; Zhao, P.; Hu, Y.; Tao, J.; Chen, J.; Huang, Y. Targeting lipid metabolism to overcome EMT-associated drug resistance via integrin β3/FAK pathway and tumor-associated macrophage repolarization using legumain-activatable delivery. *Theranostics* **2019**, *9* (1), 265−278.

(21) Colapietro, F.; Gershwin, M. E.; Lleo, A. PPAR agonists for the treatment of primary biliary cholangitis: Old and new tales. *J. Transl. Autoimmun.* **2023**, *6*, 100188.

(22) Mirza, A. Z.; Althagafi, I. I.; Shamshad, H. Role of PPAR receptor in different diseases and their ligands: Physiological importance and clinical implications. *Eur. J. Med. Chem.* **2019**, *166*, 502−513.

(23) Guo, X.; Liang, X. J.; Liu, J. L.; Li, Z. H.; You, Z.; Zhao, D.; Song, Y.; Li, L.; Song, X. Q. Precise carrier-free Pt(IV)-nanobombs for apoptosis/ferroptosis synergistic tumor therapy: A new effective method to obtain good chemotherapy and low toxicity. *J. Med. Chem.* **2025**, *68* (1), 387−404.

(24) Wang, Y.; Cai, L.; Li, H.; Chen, H.; Yang, T.; Tan, Y.; Guo, Z.; Wang, X. Overcoming cancer resistance to platinum drugs by inhibiting cholesterol metabolism. *Angew. Chem., Int. Ed.* **2023**, *62* (42), No. e202309043.

(25) Shao, X.; Zhao, X.; Wang, B.; Fan, J.; Wang, J.; An, H. Tumor microenvironment targeted nano-drug delivery systems for multidrug resistant tumor therapy. *Theranostics* **2025**, *15* (5), 1689−1714.

(26) Li, Z.; Xiao, C.; Yang, X.; Li, Z. Progress in the mechanical properties of nanoparticles for tumor-targeting delivery. *Chem. Soc. Rev.* **2025**, *54*, 5698.

(27) Wang, W.; Yang, F.; Zhang, L.; Wang, M.; Yin, L.; Dong, X.; Xiao, H.; Xing, N. Targeting DNA damage and repair machinery via delivering WEE1 Inhibitor and Platinum (IV) prodrugs to stimulate STING pathway for maximizing chemo-immunotherapy in bladder cancer. *Adv. Mater.* **2024**, *36* (1), No. e2308762.

(28) Li, X.; Cai, J.; Zhang, H.; Sun, S.; Zhao, S.; Wang, Z.; Nie, X.; Xu, C.; Zhang, Y.; Xiao, H. A trisulfide bond containing biodegradable polymer delivering Pt(IV) prodrugs to deplete glutathione and donate H_2S to boost chemotherapy and antitumor immunity. *ACS Nano* **2024**, *18* (11), 7852−7867.

(29) Liu, Y.; Wang, Q.; Yu, S.; Liu, M.; Han, J.; Sun, B. Construction and evaluation of novel dual-function antifungal inhibitors and covalent organic framework carriers based on the infection microenvironment. *J. Med. Chem.* **2023**, *66* (19), 13838−13857.

https://doi.org/10.1021/acs.jmedchem.5c01395
J. Med. Chem. 2025, 68, 20340−20359

(30) Mitra, S.; Sasmal, H. S.; Kundu, T.; Kandambeth, S.; Illath, K.; Díaz Díaz, D.; Banerjee, R. Targeted drug delivery in covalent organic nanosheets (CONs) via sequential postsynthetic modification. *J. Am. Chem. Soc.* **2017**, *139* (12), 4513−4520.
(31) Zhang, G.; Li, X.; Liao, Q.; Liu, Y.; Xi, K.; Huang, W.; Jia, X. Water-dispersible PEG-curcumin/amine-functionalized covalent organic framework nanocomposites as smart carriers for in vivo drug delivery. *Nat. Commun.* **2018**, *9* (1), 2785.
(32) Ji, S.; Wang, L.; Zhang, N. Covalent grafting synthesis of molecularly imprinted covalent organic framework for selective removal of clenbuterol from aqueous medium and milk sample. *Polymer* **2024**, *313*, 127698.
(33) Roncato, F.; Rruga, F.; Porcù, E.; Casarin, E.; Ronca, R.; Maccarinelli, F.; Realdon, N.; Basso, G.; Alon, R.; Viola, G.; et al. Improvement and extension of anti-EGFR targeting in breast cancer therapy by integration with the Avidin-Nucleic-Acid-Nano-Assemblies. *Nat. Commun.* **2018**, *9* (1), 4070.
(34) Ye, W.-L.; Zhao, Y.-P.; Li, H.-Q.; Na, R.; Li, F.; Mei, Q.-B.; Zhao, M. G.; Zhou, S. Y. Doxorubicin-poly (ethylene glycol)-alendronate self-assembled micelles for targeted therapy of bone metastatic cancer. *Sci. Rep.* **2015**, *5* (1), 14614.
(35) Chen, Y.; Feng, S.; Zhang, M.; Li, S.; Zhang, N.; Han, J.; Liu, Z.; Liu, M.; Wang, Q. Cetirizine platinum(IV) complexes with antihistamine properties inhibit tumor metastasis by suppressing angiogenesis and boosting immunity. *J. Inorg. Biochem.* **2025**, *262*, 112766.
(36) Li, Z.; Wang, Q.; Li, L.; Chen, Y.; Cui, J.; Liu, M.; Zhang, N.; Liu, Z.; Han, J.; Wang, Z. Ketoprofen and Loxoprofen platinum(IV) complexes displaying antimetastatic activities by inducing DNA damage, inflammation suppression and enhanced immune response. *J. Med. Chem.* **2021**, *64* (24), 17920−17935.
(37) Zhang, M.; Li, L.; Li, S.; Liu, Z.; Zhang, N.; Sun, B.; Wang, Z.; Jia, D.; Liu, M.; Wang, Q. Development of clioquinol platinum(IV) conjugates as autophagy targeted antimetastatic agents. *J. Med. Chem.* **2023**, *66* (5), 3393−3410.
(38) Chen, Y.; Zhang, M.; Liu, Z.; Zhang, N.; Wang, Q. Ursodeoxycholic acid platinum(IV) conjugates as antiproliferative and antimetastatic agents: Remodel the tumor microenvironment through suppressing JAK2/STAT3 signaling. *J. Med. Chem.* **2024**, *67* (19), 17551−17567.
(39) Bai, L.; Phua, S. Z.; Lim, W. Q.; Jana, A.; Luo, Z.; Tham, H. P.; Zhao, L.; Gao, Q.; Zhao, Y. Nanoscale covalent organic frameworks as smart carriers for drug delivery. *Chem. Commun.* **2016**, *52* (22), 4128−4131.
(40) Bai, L.; Wang, P.; Bose, P.; Li, P.; Zou, R.; Zhao, Y. Macroscopic architecture of charge transfer-induced molecular recognition from electron-rich polymer interpenetrated porous frameworks. *ACS Appl. Mater. Interfaces* **2015**, *7* (9), 5056−5060.
(41) Fong, G. H. Regulation of angiogenesis by oxygen sensing mechanisms. *J. Mol. Med.* **2009**, *87* (6), 549−560.

https://doi.org/10.1021/acs.jmedchem.5c01395
J. Med. Chem. 2025, 68, 20340−20359